Brain, Behavior, and Immunity 118 (2024) 380–397

Contents lists available at ScienceDirect

Brain Behavior and Immunity

journal homepage: www.elsevier.com/locate/ybrbi

Full-length Article

Anti-GluA3 autoantibodies define a new sub-population of frontotemporal lobar degeneration patients with distinct neuropathological features

Maria Italia [a], Michela Salvadè [a], Filippo La Greca [a], Elisa Zianni [a], Silvia Pelucchi [a], Alessio Spinola [a], Elena Ferrari [a], Silvana Archetti [b], Antonella Alberici [c], Alberto Benussi [c], Eino Solje [d,e], Annakaisa Haapasalo [f], Dorit Hoffmann [f], Kasper Katisko [d,e], Johanna Krüger [g,h,i], Roberta Facchinetti [j], Caterina Scuderi [j], Alessandro Padovani [c], Monica DiLuca [a], Diego Scheggia [a], Barbara Borroni [c], Fabrizio Gardoni [a,*]

[a] Department of Pharmacological and Biomolecular Sciences (DiSFeB), University of Milan, Milan, Italy
[b] Department of Laboratories, Central Laboratory of Clinical Chemistry Analysis. ASST Spedali Civili, Brescia, Italy
[c] Neurology Unit, Centre for Neurodegenerative Disorders, Department of Clinical and Experimental Sciences, University of Brescia, Brescia, Italy
[d] Institute of Clinical Medicine - Neurology, University of Eastern Finland, Kuopio, Finland
[e] Neuro Center, Neurology, Kuopio University Hospital, Kuopio, Finland
[f] A. I. Virtanen Institute for Molecular Sciences, University of Eastern Finland, Kuopio, Finland
[g] Research Unit of Clinical Medicine, Neurology, University of Oulu, Oulu, Finland
[h] Neurocenter, Neurology, Oulu University Hospital, Oulu, Finland
[i] Medical Research Center, Oulu University Hospital, Oulu, Finland
[j] Department of Physiology and Pharmacology "Vittorio Erspamer", Sapienza University of Rome, Rome, Italy

ARTICLE INFO

Keywords:
Tau
Behaviour
Positive allosteric modulators
Animal model
Personalized medicine

ABSTRACT

Autoantibodies directed against the GluA3 subunit (anti-GluA3 hIgGs) of AMPA receptors have been identified in 20%–25% of patients with frontotemporal lobar degeneration (FTLD). Data from patients and *in vitro/ex vivo* pre-clinical studies indicate that anti-GluA3 hIgGs negatively affect glutamatergic neurotransmission. However, whether and how the chronic presence of anti-GluA3 hIgGs triggers synaptic dysfunctions and the appearance of FTLD-related neuropathological and behavioural signature has not been clarified yet. To address this question, we developed and characterized a pre-clinical mouse model of passive immunization with anti-GluA3 hIgGs purified from patients. In parallel, we clinically compared FTLD patients who were positive for anti-GluA3 hIgGs to negative ones.

Clinical data showed that the presence of anti-GluA3 hIgGs defined a subgroup of patients with distinct clinical features. In the preclinical model, anti-GluA3 hIgGs administration led to accumulation of phospho-tau in the postsynaptic fraction and dendritic spine loss in the prefrontal cortex. Remarkably, the preclinical model exhibited behavioural disturbances that mostly reflected the deficits proper of patients positive for anti-GluA3 hIgGs. Of note, anti-GluA3 hIgGs-mediated alterations were rescued in the animal model by enhancing glutamatergic neurotransmission with a positive allosteric modulator of AMPA receptors. Overall, our study clarified the contribution of anti-GluA3 autoantibodies to central nervous system symptoms and pathology and identified a specific subgroup of FTLD patients. Our findings will be instrumental in the development of a therapeutic personalised medicine strategy for patients positive for anti-GluA3 hIgGs.

1. Introduction

Over the last two decades, the progressive identification of autoantibodies that target brain antigens has caught the attention of researchers, and a growing consensus is now indicating a direct pathogenic role for these autoantibodies in disorders of the nervous system. This opens new avenues in the understanding of the mechanisms associated with these pathological conditions (Duong and Prüss, 2023). It

* Corresponding author.
E-mail address: fabrizio.gardoni@unimi.it (F. Gardoni).

https://doi.org/10.1016/j.bbi.2024.03.018
Received 24 May 2023; Received in revised form 7 March 2024; Accepted 11 March 2024
Available online 12 March 2024

has been shown that many antineuronal antibodies confer pathogenicity by direct interaction with essential surface proteins, such as receptors and adhesion molecules. This interaction disturbs the physiological activity of the targeted proteins, leading to deficits in synaptic transmission, plasticity, and neuronal circuits (Hunter et al., 2021). In parallel, it has been demonstrated that antineuronal autoantibodies promote the onset of many symptoms in a variety of neuropsychiatric syndromes, including cognitive alterations, behavioural changes, dementia-like disorders, and psychosis as well as epileptic seizures and movement disorders. These discoveries suggest a reconsideration of some of these syndromes as autoantibody-related conditions for which autoantibody-directed pharmacological approaches are feasible (Duong and Prüss, 2023).

Among the variety of autoantibodies targeting ionotropic glutamate receptor subunits described in central nervous system disorders and encephalitis (*i.e.*, Rasmussen) (Gardoni et al., 2021), the specific role of antibodies against the GluA3 subunit (anti-GluA3 hIgGs) of AMPA-type glutamate receptors (AMPARs) and their association with the disease symptoms remain mostly unclear. Notably, our group has recently identified anti-GluA3 hIgGs in patients with frontotemporal lobar degeneration (FTLD) (Borroni et al., 2017; Palese et al., 2020; Scheggia et al., 2021), further supporting the hypothesis of the involvement of an immunological mechanism in the pathogenesis of this disorder (Arshad et al., 2021; Hansen, 2021; Hansen et al., 2021; Younes et al., 2018). We demonstrated that acute *in vitro* or *in vivo* treatment with anti-GluA3 hIgGs decreases GluA3 levels at synapses (Borroni et al., 2017; Scheggia et al., 2021). Similarly, patients positive for anti-GluA3 hIgGs (anti-GluA3-Ab+) exhibited reduced post-synaptic GluA3 levels in the frontotemporal cortex (Palese et al., 2020). Furthermore *in vivo* neurophysiological evaluation of glutamatergic transmission indicated impairment of intracortical facilitation in anti-GluA3-Ab+ patients, confirming the detrimental effect of anti-GluA3 autoantibodies at excitatory neurons (Palese et al., 2020). Finally, Day and colleagues recently demonstrated that the acute administration of anti-GluA3 hIgGs to hippocampal neurons mediates inhibitory effects on neuronal excitability (Day et al., 2023).

Overall, these results suggest that a deeper understanding of the role played by anti-GluA3 autoantibodies through both pre-clinical and clinical evaluation could represent a substantial improvement in the comprehension of the pathogenic mechanisms of the disease.

Analysis of the literature indicated the availability of very few chronic *in vivo* models to evaluate the toxic effects exerted by antineuronal antibodies targeting ionotropic glutamate receptors at the molecular and cellular level in the central nervous system (Haselmann et al., 2018). Consistent data are available only for pre-clinical studies addressing the role and mechanisms associated with anti-NMDA receptor (NMDAR) autoantibodies (Hunter et al., 2021).

In the present study, we developed a new mouse model by injecting anti-GluA3 hIgGs isolated from FTLD patients into C57BL/6J male mice once a week for 1 month through an intracerebroventricular cannula. *Ex vivo* analyses of mice pre-frontal cortexes (PFCs) showed that anti-GluA3 hIgGs-treated mice presented early signs of synapse loss, with a decrease in spine density and a selective accumulation of the phosphorylated form of tau in the post-synaptic compartment. In addition, we confirmed a decrease in the surface expression of GluA3-containing AMPARs. Together with these molecular and morphological abnormalities, anti-GluA3 hIgGs-treated mice exhibited impaired cognitive and affective behaviour in addition to alterations in reward-seeking behaviour and a reduction in their preference for novelty. Of note, similar symptoms along with an increase in cerebrospinal fluid (CSF) phosphorylated tau levels have been detected in anti-GluA3-Ab+ FTLD patients compared with anti-GluA3 negative FTLD patients. Finally, chronic treatment with a positive allosteric modulator (PAM) of AMPAR (S 47445) was able to rescue most of the detrimental molecular, morphological, and behavioural effects induced by anti-GluA3 hIgGs in the mouse model, thereby paving the way for a personalised pharmacological approach for anti-GluA3-Ab+ patients.

2. Methods

2.1. Human participants and clinical assessment

Patients fulfilling criteria for an FTLD syndrome were consecutively recruited from the Centre for Neurodegenerative Disorders, Department of Clinical and Experimental Sciences, University of Brescia, Italy. These syndromes included the behavioural variant of FTD (bvFTD) (Rascovsky et al., 2011), the non-fluent/agrammatic variant of primary progressive aphasia (avPPA), the semantic variant of PPA (svPPA) (Gorno-Tempini et al., 2011), corticobasal syndrome (CBS) (Armstrong et al., 2013), and progressive supranuclear palsy (PSP) (Höglinger et al., 2017). Clinical and biological characteristics of the patients are reported in Table 1. Each participant underwent a neurological evaluation, routine

Table 1
Clinical and biological characteristics of anti-GluA3-Ab + and GluA3-Ab- FTLD patients.

	GluA3+ (n = 86)	GluA3- (n = 174)	*p*-value*
Sex, female n (%)	36 (41.9 %)	72 (41.4 %)	1.000
Age at onset, years	60.9 ± 8.9	63.1 ± 8.0	0.052
Disease duration, years	2.6 ± 1.7	2.4 ± 2.0	0.388
Education, years	10.0 ± 4.3	9.3 ± 4.1	0.214
FTLD-CDR sum of boxes	4.9 ± 3.2	5.1 ± 4.8	0.702
Mini Mental State Examination	23.4 ± 6.4	23.7 ± 6.0	0.741
bvFTD/avPPA/svPPA/CBS/PSP	50/16/7/7/6	73/26/15/37/23	0.021
Frontal behavioural inventory			
Apathy	2.0 (1.0–3.0)	1.0 (0.0–2.0)	0.036
Aspontaneity	2.0 (0.0–3.0)	0.0 (0.0–2.0)	0.023
Indifference/emotional flatness	0.5.0 (0.0–2.0)	0.0 (0.0–1.0)	0.381
Inflexibility	1.0 (0.0–2.0)	0.0 (0.0–1.0)	0.012
Personal neglect	0.0 (0.0–2.0)	0.0 (0.0–1.0)	0.007
Disorganization	1.0 (0.0–2.0)	0.0 (0.0–2.0)	0.055
Inattention	1.0 (0.0–2.0)	1.0 (0.0–2.0)	0.021
Loss of insight	1.0 (0.0–2.0)	0.0 (0.0–2.0)	0.205
Logopenia	1.0 (0.0–2.0)	0.0 (0.0–2.0)	0.005
Comprehension deficit	0.0 (0.0–0.0)	0.0 (0.0–0.0)	0.189
Aphasia and verbal apraxia	1.0 (0.0–2.0)	0.0 (0.0–2.0)	0.516
Alien hand and/or apraxia	0.0 (0.0–0.0)	0.0 (0.0–0.0)	0.822
Perseveration/obsessions	0.0 (0.0–2.0)	0.0 (0.0–1.0)	0.402
Irritability	1.0 (0.0–2.0)	0.0 (0.0–2.0)	0.109
Excessive jocularity	0.0 (0.0–0.0)	0.0 (0.0–0.0)	0.649
Poor judgment and impulsivity	0.0 (0.0–2.0)	0.0 (0.0–0.0)	0.003
Hoarding	0.0 (0.0–0.0)	0.0 (0.0–0.0)	0.832
Inappropriateness	0.0 (0.0–1.0)	0.0 (0.0–0.0)	0.058
Restlessness/roaming	0.0 (0.0–0.0)	0.0 (0.0–0.0)	0.124
Aggression	0.0 (0.0–1.0)	0.0 (0.0–0.0)	0.036
Hyperorality/food fads	0.0 (0.0–2.0)	0.0 (0.0–1.0)	0.014
Hypersexuality	0.0 (0.0–0.0)	0.0 (0.0–0.0)	0.501
Utilization behaviour	0.0 (0.0–0.0)	0.0 (0.0–0.0)	0.367
Incontinence	0.0 (0.0–0.0)	0.0 (0.0–0.0)	0.179
Cerebrospinal fluid			
Total-tau	366.1 ± 281.5	321.2 ± 174.7	0.278
Phospho-tau$_{181}$	81.6 ± 119.5	47.0 ± 26.7	0.016
Amyloid beta$_{1\text{-}42}$	898.3 ± 315.9	812.5 ± 333.3	0.177

Sex is reported as n (%), demographic characteristics and CSF analysis are reported as mean ± SD, Frontal behavioural inventory scores are reported as median (interquartile range); FTLD-CDR = Frontotemporal Lobar Degeneration – Clinical dementia rating Scale; bvFTD = behavioural variant frontotemporal dementia; avPPA = agrammatic variant Primary Progressive Aphasia; svPPA = semantic variant Primary Progressive Aphasia; CBS = Corticobasal Syndrome; PSP = Progressive Supranuclear Palsy.
*Demographic characteristics and CSF analysis are compared with one-way ANOVA or Fisher's Exact test; Frontal behavioural inventory scores are compared with a non-parametric ANCOVA (Quade's test), correcting for age and disease duration.

laboratory examination and a standardized neuropsychological and behavioural assessment, as previously reported (Benussi et al., 2019). In all FTLD cases, the diagnosis was supported by routine brain structural imaging, while CSF concentrations of tau, p-tau$_{181}$ and amyloid beta (A$\beta_{1\text{-}42}$) or PET amyloid were measured in a subset of cases, to rule out Alzheimer's disease, as previously reported (Borroni et al., 2015). At baseline, patients underwent a standardized neuropsychological battery which included the mini-mental state examination (MMSE), the Rey auditory verbal learning test (immediate and delayed recall), the Rey complex figure (copy and recall), the digit span, phonemic and semantic fluencies, the token test, the clock-drawing test, and the trail-making test (part A and part B) (Cosseddu et al., 2018). The level of functional independence was assessed with the basic activities of daily living (BADL) and the instrumental activities of daily living (IADL) questionnaires, whereas neuropsychiatric and behavioral disturbances were evaluated with the frontal behavior inventory (FBI) (Cosseddu et al., 2020; Kertesz et al., 1997). Disease severity was assessed using the global CDR plus NACC FTLD (Knopman et al., 2008; Miyagawa et al., 2020). Disease duration was measured as the onset of first reported symptoms by the patient or caregiver, and the clinical evaluation.

For all participants, informed consent in the study was obtained according to sampling protocols that were approved by the Ethics Committee of Brescia Hospital, Italy. The study was conducted in accordance with the Helsinki Declaration.

2.2. Mice

All procedures were approved by the Italian Ministry of Health and the local Animal Use Committee (projects n° 1161–2020, 182–2022) and were conducted in accordance with the Guide for the Care and Use of Laboratory Animals of the National Institutes of Health and the European Community Council Directives. Routine veterinary care and animal maintenance were provided by dedicated and trained personnel. Two- to three-month-old male C57BL/6J animals were used. Animals were housed two per cage in a climate-controlled facility (22 ± 2 °C, humidity 45–65%), with ad libitum access to food and water throughout, and with a 12 hours light–dark cycle (19:00 07:00 schedule). Experiments were run during the light phase (between 10:00–17:00). All mice were handled on alternate days during the week preceding the first behavioural testing.

2.3. Experimental design

For pre-clinical evaluations, no statistical methods were used to predetermine sample size for single experiments. The animal numbers were based on estimations from previous studies, including our own published studies (Ferretti et al., 2019; Haselmann et al., 2018; Scheggia et al., 2020). Outliers were identified using ROUT (Q = 1%) method. In addition, we excluded from data collection all the mice that showed behavioural signs of distress. We used different cohorts of mice for different tasks and analyses only when we expected that a certain task would have influenced the outcome of the subsequent one. Conversely, when it was possible, we used the same cohort of mice for different tasks and analyses. The same sample was not measured repeatedly. For all the tests, littermates were randomly assigned to the different groups. Experimenters were not blinded during data acquisition, but all analyses were performed with blinding of the experimental conditions.

2.4. Serum dosage and purification of anti-GluA3 antibody from FTLD patients

Serum samples were frozen immediately after centrifugation and stored at −80 °C before enzyme-linked immunosorbent assay. The detection of anti-GluA3 antibodies was performed by enzyme-linked immunosorbent assay (ELISA) according to a previously published protocol (Borroni et al., 2017; Mantegazza et al., 2002). In the ELISA assay, we used as negative control microwells coated with no peptide. Affinity purification protocol of anti-GluA3 hIgGs from FTLD patients' serum was performed by sulfo-link affinity chromatography as previously reported (Scheggia et al., 2021). As a result of the purification protocol, we obtained purified anti-GluA3 hIgGs with a final concentration of about 0,3 μg/μl. We purified anti-GluA3 hIgGs from a pool of twenty patients previously identified as positive for the autoantibodies in the ELISA assay. Both the detection and the purification were performed using a peptide with following aminoacidic sequence: NEYERFVPFSDQQISNDSASSENRT (GluA3 peptide B, amino acids 399–424, in GluA3 extracellular domain), as previously reported (Borroni et al., 2017; Scheggia et al., 2021).

2.5. In vitro validation of purified anti-GluA3 hIgGs binding to GluA3 subunit

Once purified, anti-GluA3 hIgGs were tested for their specificity for GluA3 subunit by using well-validated cell-based assays. Firstly, we verified that purified anti-GluA3 hIgGs specifically recognize GluA3 subunit using them as primary antibodies in an immunocytochemical assay (ICC). With this aim, we over-expressed a GFP-tagged human GluA3 (GFP-hGluA3, from Origene) plasmid into a non-neuronal immortalized cell line (HEK293) and we showed that purified anti-GluA3 hIgGs (but not CTRL hIgGs) specifically recognized the over-expressed GluA3 subunit. More in detail, the signal of the over-expressed GFP-hGluA3 (*green signal*) was non-nuclear and overlapped the one obtained using anti-GluA3 hIgGs as primary antibody (Fig. S1A, *magenta signal, anti-hIgGs line and anti-GluA3 hIgGs* column in the figure). Conversely, using CTRL hIgGs as primary antibody, the staining was very faint, a-specific and ubiquitously distributed into the cells over-expressing GFP-hGluA3 (Fig. S1A, *magenta signal, anti-hIgGs line and CTRL hIgGs* column in the figure). Similarly, purified anti-GluA3 hIgGs were tested for specifically binding over-expressed GFP-hGluA3 in rat primary hippocampal neurons (Fig. S1B). Moreover, to evaluate whether the purified antibodies also bind endogenous GluA3, we used anti-GluA3 hIgGs as primary antibody on primary hippocampal neurons obtaining a punctate signal along dendrite that resembled the one proper of ionotropic glutamate receptor subunits (Fig. S2A, *anti-GluA3 hIgGs column*). Conversely, the signal obtained using CTRL hIgGs as primary antibodies was a-specific and prevalently nuclear (Fig. S2A, *CTRL hIgGs* column).

Furthermore, to prove anti-GluA3 hIgGs' capability to bind GluA3 native protein on the cellular surface, we first verified that purified anti-GluA3 hIgGs bind GluA3 subunit in **live** unfixed, unpermeabilized HEK293 cells overexpressing GFP-hGluA3. Specifically, we incubated HEK293 with anti-GluA3 hIgGs (at a concentration of 0,18 ng/μl) to allow anti-GluA3 hIgGs to recognize and bind GluA3 protein. Then, we immunolabelled cells using a secondary fluorescent antibody recognizing the constant portion of hIgG. In HEK293 overexpressing GFP-hGluA3, the staining corresponding to anti-GluA3 hIgGs (Fig. S3A, *magenta channel, anti-hIgGs line and first column* in the figure) was overlapped with the one of the over-expressed hGluA3 subunit (Fig. S3A, *green channel, GFP-hGluA3 line and first* column in the figure). Notably, the pre-incubation of anti-GluA3 hIgGs with peptide B, but not with a scramble peptide (RYNEADQSPFNSQVEDRNSSIFEST) prevented the binding of anti-GluA3 hIgGs to GluA3 (Fig. S3A, *magenta channel, anti-hIgGs line and + Peptide B* or *+ Peptide Scr* columns in the figure).

Finally, we confirmed the capability of anti-GluA3 hIgGs to bind endogenous GluA3 native protein on the cellular surface also in untransfected primary hippocampal neurons. As shown in Fig. S3B, incubation of anti-GluA3 hIgGs in live unfixed, unpermeabilized primary neurons produced a punctate staining resembling dendritic spines' localization (Fig. S3B, *orange channel*), as expected for a receptor's subunit.

2.5.1. HEK293 cells over-expressing GluA3 subunit

HEK293 cells were cultured in High Glucose Dulbecco's Modified Eagle's Medium (DMEM High Glucose w/L-Glutamine w/Sodium Pyruvate ECM0728L Euroclone) supplemented with 10% Fetal Bovine Serum (Euroclone) and penicillin–streptomycin (ECB3001D, Euroclone). The day before transfection, HEK293 cells were plated in a 12-wells multiwell plate. Transfection of hGluA3-GFP (2 μg DNA/well) was carried out with lipofectamine method (Lipofectamine LTX and Plus reagent, 15338-100, Invitrogen).

2.5.1.1. Anti-GluA3 hIgGs as primary antibodies in ICC assay on HEK293 cells. 12 hours after transfection, HEK293 cells were fixed with 4% Paraformaldehyde (PFA)-4% sucrose in PBS solution for 10 min at 4 °C and then permeabilized with 0.1% Triton-X-100 in PBS for 10 min at room temperature (RT). After blocking in 5% BSA in PBS for 45 min at RT, cells were incubated with anti-GFP (chicken anti-GFP Millipore, 1:300, ABB16901) and with purified anti-GluA3 hIgGs or CTRL hIgGs (4,7 ng/μl) in 5% BSA in PBS overnight at 4 °C. Cells were then washed in PBS and incubated with proper fluorescent secondary antibodies (goat anti-chicken-Alexa488, goat anti-human-Alexa555) in 5% BSA in PBS for 1 h at RT. We finally performed nuclei staining with the fluorescent dye 4′,6-diamidino-2-phenylindole (DAPI; 1:50,000 in PBS; Thermo Fisher Scientific) for 10 min in PBS at RT. After washes in PBS coverslips were mounted on glass slides with Fluoromount mounting medium (Sigma-Aldrich).

2.5.1.2. Detection of anti-GluA3 hIgGs bound to GluA3 subunit in live HEK293. 12 hours after transfection, HEK293 were incubated with anti-GluA3 hIgGs for 30 min at 37 °C. For the experiment with peptide B and scramble peptide, anti-GluA3 hIgGs were pre-incubated for 5 min at 37 °C with peptide B or peptide scramble at a molar ratio anti-GluA3 hIgGs:peptide 1:10. After washes with D-PBS, HEK293 cells were fixed with 4% Paraformaldehyde (PFA)-4% sucrose in PBS solution for 10 min at 4 °C. After blocking in 5% BSA in PBS for 45 min at RT, cells were incubated with goat anti-human-Alexa555 in 5% BSA in PBS overnight at 4 °C. Cells were then washed in PBS and we finally performed nuclei staining with the fluorescent dye 4′,6-diamidino-2-phenylindole (DAPI; 1:50,000 in PBS; Thermo Fisher Scientific) for 10 min in PBS at RT. After washes in PBS coverslips were mounted on glass slides with Fluoromount mounting medium (Sigma-Aldrich).

2.5.2. Rat primary hippocampal neurons over-expressing (or not) GluA3 subunit

Hippocampal neuronal primary cultures were prepared from embryonic day 18 rat hippocampi as described previously (Piccoli et al., 2007). Neurons were eventually transfected on day *in vitro* 10 (DIV10) with GFP-hGluA3 (over-expression experiment) through the calcium-phosphate method.

2.5.2.1. Anti-GluA3 hIgGs as primary antibodies in ICC assay on primary hippocampal neurons. At DIV13, neurons were fixed with 4% Paraformaldehyde (PFA)-4% sucrose in PBS solution for 10 min at 4 °C and permeabilized with 0.1 % Triton-X-100 in PBS for 15 min at room temperature (RT). After blocking in 5% BSA in PBS for 45 min at RT, cells were incubated with purified anti-GluA3 hIgGs or CTRL hIgGs (4,7 ng/μl) (eventually chicken anti-GFP, over-expression experiment) overnight at 4 °C. Cells were then washed in PBS and incubated with proper fluorescent secondary antibodies (goat anti-human-Alexa555 and, eventually, goat anti-chicken-Alexa488 for over-expression experiment) for 1 h at RT. After washes in PBS coverslips were mounted on glass slides with Fluoromount mounting medium (Sigma-Aldrich).

2.5.2.2. Detection of anti-GluA3 hIgGs bound to GluA3 sub-unit in live neurons. At DIV13, neurons were incubated with anti-GluA3 hIgGs for 1 h at 37 °C. Then, ICC was performed as described for HEK-293 experiment (2.5.1.1).

For both HEK293 and neurons IHC, images were acquired with LSM900 confocal microscope (Zeiss) with a 63X objective.

2.6. Surgical procedures

To chronically administer hIgGs to mice, we used an intracerebroventricular cannula (Bilaney, Mouse guide cut 1.5 mm below pedestal, C315GS-4/Spc). To implant the cannula, C57BL/6J male mice were anesthetized with a mix of isoflurane (2%) and oxygen (1.5%) by inhalation and mounted onto a stereotaxic frame (Kopf Instruments) linked to a digital micromanipulator. Brain coordinates of intracerebroventricular cannula positioning were chosen in accordance with the mouse brain atlas: anterior–posterior (AP): −0.34 mm; medial–-lateral (ML): ±1 mm; and dorsal–ventral (DV): −2.5 mm. Once positioned, the cannula was fixed on mice skull through dental cement (Super bond universal sun medical kit dx, 410446782). Surgical procedure lasted about 30 min for each animal. Mice received carprofen (5 mg/kg) in drinking water for three consecutive days after the surgery. Through the cannula, intracerebroventricular administration of control (CTRL) hIgGs or anti-GluA3 hIgGs was performed once a week for four consecutive weeks. CTRL hIgGs are a pool of commercial human immunoglobulins (R&D Systems, cat. #1–001-A). Specifically, each animals received 2 μl of anti-GluA3 hIgGs or CTRL hIgGs at a concentration of 0,12 μg/μl. The hIgGs were infused through an injector (Bilaney, Mouse internal fits 1,5mm guide with 1 mm projection, C315IS-4/Spc) connected to a 50 μl Hamilton syringe.

2.7. Evaluation of hIgGs bound to mice brains

For determination of hIgGs bound to brain tissue using immunofluorescence, we perfused animals that received intracerebroventricular injection of either saline, CTRL hIgGs or anti-GluA3 hIgGs, with cold 4% paraformaldehyde (PFA) in 0.1 M phosphate buffered saline (PBS). The brains were then removed from the skull and post-fixed in 4% PFA in PBS for 24 h at 4°C. Then, the brains were cryoprotected with 30% sucrose in PBS1X for 48 h at 4 °C, flash-frozen with cold isopentane and stored at −80 °C. Brain sections were cut at 15 μm thickness using a cryostat at −20 °C. These sections were used for determination of the amount of hIgGs bound in situ through immunofluorescence. Specifically, the sections were rinsed gently with PBS1X and then permeabilized with 0.3% Triton X-100 in PBS (0.3% T-PBS) for 1 h at RT. After permeabilization, brain slices were blocked with 0.1% Triton X-100 in PBS (0.1% T-PBS) supplemented with 10% normal goat serum (NGS) for 2 hours at RT. After permeabilization and blocking, slices were incubated with goat anti-human-Alexa488 IgG (A11013, Invitrogen, diluted 1:1000) or goat anti-human-Alexa555 IgG (A21433, Invitrogen, diluted 1:1000) in 0.1% T-PBS supplemented with 3% NGS for one overnight (o/n) at 4 °C followed by nuclei staining with the fluorescent dye 4′,6-diamidino-2-phenylindole (DAPI; 1:50,000 in PBS; Thermo Fisher Scientific). Slices were mounted on glass slides with Fluoromount mounting medium (Sigma-Aldrich) for confocal imaging. Images were taken using LSM900 (Zeiss) confocal microscopes with alternatively 2.5X or 20X objectives. Animals infused with anti-GluA3 hIgGs, but not CTRL hIgGs or saline (data not showed for saline), had a clear human IgG immunostaining (representing human IgG bound to brain). More in detail, the human IgG immunostaining (anti-hIgGs) was evident throughout the brain, including the hippocampus (Fig. S4A) and the PFC (Fig. S4B). Of note, as showed in Fig. S4A, we obtained a similar staining using secondary anti-hIgGs conjugated to alternatively Alexa Fluor555 (left block of images) and 488 (right block of images). Overall, with these experiments, we verified the specific binding of anti-GluA3 hIgGs (but not CTRL hIgGs) to mice brains.

2.8. S 47445 administration

S 47445 (also known as CX-1632 and Tulrampator, MedChemExpress, HY-109046), a positive allosteric modulator (PAM) of AMPAR, was administrated daily through intraperitoneal injections from day 15 to day 29. The side of the injection was changed every day. According to its datasheet, S 47445 was dissolved in 10% Dimethyl sulfoxide (DMSO, Sigma-Aldrich, 276855), 40% poly(ethylene glycol)300 (PEG 300, Sigma-Aldrich, 81162), 5% Tween 80 (Sigma-Aldrich, P4780), 45% saline. On the basis of previous pre-clinical studies, we administered S 47445 at a dose of 3 mg/kg for a final volume of 100 μl. As negative control, mice were injected with the emulsion used to solve S 47445 (10% DMSO, 40% PEG 300, 5% Tween 80, 45% saline).

2.9. Subcellular fractionation

Total homogenate and Triton insoluble postsynaptic fractions (TIF) were isolated from adult mouse PFC as previously reported (Mellone et al., 2019). After measuring protein concentration, all samples were standardized at 1 mg/mL concentration.

2.10. Western blot (WB) analysis

WB analysis was performed in total homogenate and in TIF purified from mouse PFC and hippocampus and in BS3 samples. Protein samples were separated on an acrylamide/bisacrylamide gel at the appropriate concentration depending on their molecular weight. Nitrocellulose membranes (Biorad) were developed with electrochemiluminescence reagents (Biorad) and scanned with a Chemidoc (Biorad Universal Hood III). Images were quantified with computer-assisted imaging (Image Lab, Biorad). Protein levels were expressed as relative optical density (OD) measurements normalized to a housekeeping protein.

2.11. Immunohistochemistry (IHC)

Mice were perfused with cold 4% paraformaldehyde (PFA) in 0.1 M phosphate buffered saline (PBS). The brain was removed from the skull and post-fixed in 4% PFA in PBS for 1 h at 4 °C. The brain was sliced into 50 μm coronal sections using the Vibratome 1000 Plus Sectioning System (3 M). Brain slices were permeabilized in 0.3% Triton X-100 in PBS (0.3% T-PBS) for 1 h at RT, shaking. After permeabilization, brain slices were blocked with 0.1% Triton X-100 in PBS (0.1% T-PBS) supplemented with 10% normal goat serum (NGS) for 2 hours at RT, shaking. After permeabilization and blocking, slices were incubated with primary antibodies in 0.1% T-PBS supplemented with 3% NGS for 3 overnights (o/n) at 4 °C, shaking. The appropriate Alexa Fluor-conjugated secondary antibodies in 0.1% T-PBS with 3% NGS were applied for 2 hours at RT, shaking, followed by nuclei staining with the fluorescent dye 4′,6-diamidino-2-phenylindole (DAPI; 1:50,000 in PBS; Thermo Fisher Scientific). Slices were mounted on glass slides with Fluoromount mounting medium (Sigma-Aldrich) for confocal imaging. To count Iba1 and CD68 positive cells, Z-stacks of 3 μm step (for a final Z distance of 12 μm) were taken with LSM900 confocal microscope (Zeiss) with a 20X objective at 0.2 μm pixel size and analysed automatically using Fiji (ImageJ) software. To perform Sholl analysis on Iba1+ cells, Z-stacks of 0.45 μm step were taken using LSM900 (Zeiss) confocal microscopes with 63X objective at 0.09 μm pixel size and analysed using ImageJ software. Specifically, we employed the Simple Neurite Tracer plugin indicating 5 μm as radius step size. The number of intersections was plotted as a function of the radial distance from the cell soma and the total length expressed the sum of the length of the cell's ramification.

2.12. Antibodies

The following primary antibodies were used:

- mouse anti-GluA3 (MAB5416, Millipore; dilution: 1:1000 WB)
- mouse anti-GluA2 (75-002, Neuromab; dilution: 1:2000 WB)
- rabbit anti-GluA1 (13185S, Cell Signalling; dilution: 1:1,000 WB)
- rabbit anti-GluN2A (M264, Sigma; dilution: 1:1000 WB)
- rabbit anti-GluN2B (14544S, Cell Signalling; dilution: 1:1000 WB)
- mouse anti-phospho tau (MN1020, Invitrogen; dilution: 1:1000 WB)
- rabbit anti-phosphoTDP43 (22309-1-AP, Proteintech; dilution: 1:5000 WB)
- rabbit anti-human-tau (A0024, Dako; dilution: 1:1000 WB)
- rabbit anti-CD11b,c (bs-1014R, BIOSS; dilution: 1:1000 WB)
- rat anti-CD68 (1957, Biorad; dilution: 1:400 IHC)
- rabbit anti-Iba1 (019-19741, Fujifilm; dilution 1:700 IHC)
- mouse anti-actin (A5441, Sigma; dilution: 1:5000 WB)
- mouse anti-tubulin (T9026, Sigma-Aldrich; dilution: 1:5000 WB)
- chicken anti-GFP (ABB16901, Millipore; dilution: 1:300 ICC)

The following secondary antibodies were used:

- goat anti-mouse-HRP (172–1011, Bio-Rad)
- goat anti-rabbit-HRP (170–6515, Bio-Rad)
- goat anti-rabbit-Alexa488 (A-11034, Invitrogen)
- goat anti-rat-Alexa488 (A11006, Invitrogen)
- goat anti-rabbit-Alexa555 (A21428, Invitrogen)
- goat anti-human-Alexa 488 IgG (A11013, Invitrogen; dilution 1:1000 IHC)
- goat anti-human-Alexa555 (A-21433, Invitrogen; dilution 1:1000 IHC)

2.13. Cross-linking assay

Mice were sacrificed by cervical dislocation and the brains were immediately transferred into artificial cerebrospinal fluid (aCSF) (NaCl 120 mM, KCl 2.5 mM, NaHCO3 26 mM, NaH2PO4 1.24 mM, CaCl2 2 mM, MgSO4 2 mM, D-glucose 10 mM, water; pH = 7.4/7.5) previously treated with carboxigen and maintained cold in ice. Coronal slices of 200 μm of thickness containing PFC were obtained with the Vibratome 1000 Plus sectioning system (3 M). Slices were treated with 1 mg/ml (Bis (Sulfosuccinimidyl) suberate (BS3, 21580, Thermo scientific) solved in aCSF for 30 min at 4 °C in presence of carboxigen. BS3-treated slices underwent quenching in glycine (HelloBio, HB0299) 100 mM for 10 min at 4 °C. Control slices were maintained in cold aCSF in presence of carboxigen. BS3 treated and control slices were separately centrifugated at 13000 rpm for 2 min at 4 °C. The pellets were frozen and finally resuspended with Lysis buffer (NaCl 500 mM, HEPES pH 7.4 25 mM, DTT 1 mM, EDTA 2 mM, PMSF 1 mM, NaF 20 mM, NONIDET P-40 0.10%, water; pH = 7.4/7.5) with protease inhibitor 1X (Complete, GE Healthcare) and phosphatase inhibitor 1X (PhosSTOP, Roche Diagnostics GmbH) in a glass-glass potter. After measuring protein concentration, all samples were standardized at 1 mg/mL concentration in and then analysed through western blot analysis. BS3 does not cross cell membranes so it covalently crosslinks cell surface expressed receptors while intracellular receptors are not modified enabling surface and intracellular receptor pools to be distinguished and measured. Quantitative analysis was performed as a comparison between the portion of slices treated with BS3 (BS3+ -treated slices) and the portion of the slices from the same animal not treated with BS3 (CTRL slices).

2.14. Spine morphology

Carbocyanine dye DiI (D282, Invitrogen) was used to label neurons as previously reported (Kim et al., 2007; Scheggia et al., 2021; Stanic et al., 2015). Z-stacks of 0.45 μm steps were taken with a confocal microscope (Zeiss) and analysed using Fiji (ImageJ) software. Specifically, for each dendritic spine, spine length, width and neck were manually measured at selected regions of interest. These measurements were used to classify dendritic spines into three categories (thin, stubby, and

mushroom) (see also (Gardoni et al., 2012; Harris et al., 1992; Scheggia et al., 2021)). For each neuron, an average of 3 dendrites that are distant from the neuron soma no more than 200 μm, for a total dendritic length of about 200–300 μm, was considered. For spine morphology studies, we analysed brain samples only from mice that did not undergo behavioural and cognitive tests. To avoid issues related to a possible different effect of the Abs on the two sides, confocal imaging was performed on a balanced number of stained neurons of the two hemispheres.

2.15. Open field (OF)

To assess general locomotor activity, mice were individually placed in the centre of the open field arena (Ugo Basile, 44 × 44 cm) and video-tracking software (ANY-maze 6.2, Stoelting) was used to record and analyse their movements for one hour. The distance travelled and the time spent at the centre and the corners of the arena were automatically calculated by the ANY-maze software.

2.16. Rotarod task

To assess motor learning, coordination and balance, mice were tested on a rotarod apparatus (Ugo Basile) as described by Ferrari and colleagues (Ferrari et al., 2022). To familiarize them with the instrument, each mouse was given training sessions (three trials/day for a maximum of 300 s/trial) for 3 days before the testing days. Each test session was composed of three consecutive trials of the duration of maximum 300 s with 2 min as inter-trial interval; the trial was stopped as the mouse fell off the rotarod bar. For the accelerating rotarod test, each mouse was placed on the rotarod with the speed increasing from 4 rpm to 40 rpm. The latency to fall off the rotarod bar was recorded for each mouse in each test and the mean of the duration of three consecutive trials was used for the analysis.

2.17. Elevated plus maze

Mice were tested in the elevated plus maze to assess anxiety-like behaviour (Walf and Frye, 2007). Mice were placed in the maze at the junction of the four arms (*i.e.*, two open and two enclosed arms, Ugo Basile), and entries and duration in each arm were recorded by a video-tracking system (Anymaze 6.2, Stoelting) for 5 min.

2.18. Novel object recognition task (NORT)

The procedure for the novel object recognition task was adapted from a previous study (Barker and Warburton, 2011) as described by Scheggia and colleagues (Scheggia et al., 2021). Mice were tested in a standard open field arena (Ugo Basile, 44 × 44 cm) with black Polyvinyl chloride (PVC) walls to which were habituated for 1 h the day before testing. The stimuli were objects constructed from Duplo blocks (Lego) and varied in shape, colour, and size, and were too heavy to be displaced. The task consists of an acquisition phase (10 min) and a recognition test (5 min), separated by a 5-minute delay. During the acquisition phase, the mice were placed in the area with two identical objects and allowed to explore. During the test, one of the two objects was replaced with a novel object. The positions of the objects in the test and the objects used as novel or familiar were counterbalanced between the animals. During the delay period, all the objects were cleaned with alcohol to remove olfactory cues and any sawdust that had stuck to the object. To express the discrimination between the objects, we calculated a discrimination ratio as the absolute difference in the time spent exploring the novel object and the familiar object divided by the total time spent exploring the two objects.

2.19. Affective discrimination task (ADT)

This task was adapted from previous studies (Ferretti et al., 2019; Scheggia et al., 2020) as described by Scheggia and colleagues (Scheggia et al., 2021).

2.20. Free reward consumption task

As habituation to the experimental setting, the day before the task, mice were placed individually in empty standard mouse cages for one hour. On the day of the task (performed in the same room and in the same cages of the habituation), mice were left individually in the cages with 50 pellets of palatable food (14 mg, Test Diet, 5-TUL) for 2 hours. The number of pellets eaten was monitored over time. The result of the task was expressed as number of pellets eaten (50 - pellet/s left in the cage) at the end of the two hours. We tested mice both after a period of food restriction, to stimulate their interest in food consumption, and in satiety.

2.21. Food seeking task

Food seeking task was performed in a standard operant chamber (length of 24 cm × width of 20 cm × height of 18.5 cm; ENV-307 W-CT, Med Associates). A food magazine connected to an external dispenser of food pellets was available in the centre of the operant chamber and two circular holes (*i.e.*, nose-poke holes) were located on the food magazine's right and left respectively. Mice were mildly food restricted to 85–90% of their free-feeding body weights to promote food-seeking behaviour. Each session lasted 40 min. Before the beginning of the test, every operant box was cleaned with ethanol 50%. During the task, mice were individually positioned in a single operant chamber where their movements were monitored by custom scripts written in MED-PC V (Med Associates). First, mice had to associate the insertion of the nose in one of the two nose-poke holes with the delivery of the food reward pellet(s) in the magazine. The number of nose-pokes required to obtain one food reward pellet represents the fixed ratio. The nose-poke hole that allowed the delivery of the food reward pellet(s) in the food magazine, represented the active nose-poke hole. The other nose-poke hole did not produce any effect and represented the inactive one. We named the choice of the active nose-poke hole as "Food-related response" and the choice of the inactive nose-poke hole as "Non-food related response". The location of the Food-related response was counterbalanced between left and right nose-pokes across mice to avoid position bias. Once assigned in the habituation phase, however, the position of the Food-related response never changed across test sessions of the same mouse. The habituation continued until all the mice understood the task. This was indicated by a positive preference index, calculated as the number of food-related responses – the number of non-food related responses / the total number of responses. Generally, mice took two days to understand the task. Once habituated, we measured mice task performance by measuring the preference index, the total number of food-related responses, the total number of responses and the time interval between a food-related response and the subsequent one (*i.e.*, average food latency). We tested mice both after a period of food restriction, to stimulate their interest in food seeking, and in satiety. Mice were tested both with a fixed ratio = 1 and a fixed ratio = 4 or 8.

2.22. Sucrose preference task

Sucrose Preference Task was partially adapted from the protocol of Amodeo and colleagues (Amodeo et al., 2021). As habituation to the experimental setting, mice were placed individually in cages with two drinking bottles both containing water for 12 hours. Then, after a night in their original cages, mice were re-placed individually in the same cages of the habituation with a bottle containing water and another with 1% sucrose solution (Sigma-Aldrich, 84097). During the test, mice had free access to the two bottles for 24 h. The two bottles were not visibly distinguishable and were both weighed before, after 12 hours and at the end of the test. The two bottles were also switched in their position after

12 hours to avoid position bias in drinking behaviour. Sucrose preference was calculated as the percentage of the volume of sucrose intake over the total volume of fluid intake for each tested animal.

2.23. Quantification and statistical analysis

Mice experiments: All the group values are expressed as mean ± s.e.m. Comparisons between groups were performed using the following tests as appropriate: two-tailed unpaired Student's t test, Mann–Whitney test, ordinary one-way ANOVA, Kruskal-Wallis test and 2-way ANOVA. Statistical analyses were performed using the GraphPad Prism statistical package (GraphPad software). Number of neurons and mice used as well as all the statistical details of experiments are reported in the figure legends. Normal distribution was checked using D'Agostino & Pearson normality test or by using Shapiro-Wilk normality test when n was insufficient.

Patients: Continuous and categorical variables are reported as mean ± standard deviation or numbers (%). Biological and clinical features were compared between patients with and without anti-GluA3-Ab+ by ANCOVA analysis, corrected for age and disease duration, while behavioural measures were compared by a non-parametric ANCOVA (Quade's test), corrected for age and disease duration. A two-sided p-value < 0.05 was considered significant and corrected for multiple comparisons using the Benjamini-Hochberg false discovery rate (FDR) (Benjamini and Hochberg, 1995). Data analyses were carried out using IBM SPSS software (version 29.0).

3. Results

3.1. Chronic anti-GluA3 hIgGs administration induced a reduction in GluA3-containing AMPAR surface retention and the appearance of early signs of synapse loss and tau phosphorylation

To evaluate the effects of chronic anti-GluA3 hIgGs administration, we injected male mice in the lateral ventricles once a week for 1 month (on days 1, 8, 15, and 22) with anti-GluA3 hIgGs that were isolated from FTLD patients (Fig. 1A). As a control, mice were injected with a pool of human immunoglobulins (CTRL hIgGs).

Numerous studies (Haselmann et al., 2018; Hughes et al., 2010; Lai et al., 2009; Maudes et al., 2022; Mikasova et al., 2012; Peng et al., 2015) reported that pathogenic IgG antibodies targeting extracellular epitopes of membrane receptors often promote the endocytosis of the receptor itself. By employing a crosslinking assay of surface proteins, we found that chronic anti-GluA3 hIgGs injection mediated an increase in the intracellular levels of GluA3 and GluA2 subunits (Fig. 1B, C) and consequently decreased their surface retention. Interestingly, we did not detect any differences in the levels of the subunits in a purified triton-insoluble post-synaptic fraction (TIF) (Fig. 1B, D). This suggests that anti-GluA3 hIgGs induce an endocytic process of GluA3-containing AMPARs within the dendritic spine compartment. The surface insertion of other subunits of ionotropic glutamate receptors (*i.e.*, GluA1, GluN2A, and GluN2B) was unaffected by chronic anti-GluA3 hIgGs injection (Fig. S5A, B). Overall, these data indicate that anti-GluA3 hIgGs selectively target GluA2/GluA3 AMPAR heteromers, affecting their correct retention into the synaptic membrane.

Tau protein and TDP43 are the most frequently identified proteinopathies in frontotemporal dementia (Mackenzie et al., 2010). Recent studies have indicated that tau hyperphosphorylation (p-tau) promotes tau migration into the post-synaptic compartment. In this compartment, p-tau negatively affects the synapses' functionality, interfering with ionotropic glutamate receptors (Italia et al., 2022). We measured the levels of tau and its hyperphosphorylated form in the post-synaptic compartment and in the total homogenate isolated from mice PFCs. We found selective accumulation of the p-tau (Ser202, Thr205) at post-synaptic sites (Fig. 1E, F) but not in the total homogenate of anti-GluA3 hIgGs-treated mice (Fig. S5C, D). Furthermore, we did not detect any differences in total tau or pTDP43 levels in the post-synaptic fraction or in the total homogenate following anti-GluA3 hIgGs administration (Figs. 1E, F; S5C, D). This last result suggests the specific involvement of tau-related pathological intracellular cascades in anti-GluA3 hIgGs-treated mice.

Having detected selective accumulation of p-tau in the post-synaptic compartment and altered GluA3-containing AMPAR retention in the membrane of anti-GluA3 hIgGs-treated mice, we hypothesised that these events could negatively influence dendritic spines' morphology and structure. *Ex-vivo* spine morphology analysis revealed that mice chronically infused with anti-GluA3 hIgGs were characterised by a significant decrease in dendritic spine density in the PFC (Fig. 1G, H). For a more detailed morphological analysis, we measured dendritic spine's length and head and neck width, which allowed spine categorisation according to shape (mushroom, stubby, or thin). However, no differences in spine length or head width were found between anti-GluA3 hIgGs-treated mice and CTRL hIgGs-treated mice (Fig. 1I, J); accordingly, no differences in the relative percentage of spine subtypes were detected (Fig. S5E).

Altogether, these results indicate that the chronic presence of anti-GluA3 hIgGs leads to synapse loss that may represent an early sign of a neurodegenerative process.

We further investigated whether the presence of anti-GluA3 hIgGs could trigger a neuroinflammatory process. We evaluated microglial status and activation. First, we analysed the expression of Iba1, a Ca^{2+}-binding protein constitutively expressed by both surveillant and activated microglia, and CD11b and CD68, two markers of microglial activation in the mouse PFC. Through immunohistochemical analysis, we quantified the number of Iba1+ cells and their average size (Fig. S6B, C), and we evaluated the expression of CD68 (Fig. S6D). Furthermore, we investigated the complexity of Iba1+ arborisation through Sholl analysis (Fig. S6F, G). Finally, we analysed CD11b/c levels in total homogenate obtained from mice PFCs (Fig. S6I). None of these parameters were affected by anti-GluA3 hIgGs administration with the exception of the mean area of Iba1+ cells, which appeared to be larger in anti-GluA3 hIgGs-treated mice (Fig. S6C). Accordingly, anti-GluA3 hIgGs administration did not mediate profound alterations in microglial status.

3.2. Anti-GluA3 hIgGs administration reduced interest for novelty

To evaluate the *in-vivo* effects of chronic anti-GluA3 hIgGs administration, we first measured the locomotor activity of the mice in an open field (OF) arena, and we observed that the anti-GluA3 hIgGs-treated mice exhibited a reduction in the total distance travelled compared with CTRL mice (Fig. 2A). Because this effect could be related to reduced propensity to explore the environment, we stimulated exploration by introducing two identical objects in the OF. Despite this, anti-GluA3 hIgGs-treated mice still showed reduced locomotor activity in the OF (Fig. 2B). We did not observe any motor impairments in the Rotarod task (Fig. S7A) or anxiety-like behaviour in the Elevated Plus Maze (Fig. S7B, C) and in the OF arena (Fig. S7D). Therefore, we hypothesised that anti-GluA3 hIgGs administration could result in reduced interest in exploration.

To further investigate this finding, we evaluated mice via the Novel Object Recognition Task (Fig. 2C), which measures the capability of mice to discriminate between a familiar and a newly presented object. The introduction of a new object represents an even stronger stimulus to motivate exploration in mice. In addition, the capability to recognise the new object requires the functioning of higher cortical areas, including the PFC (Barker and Warburton, 2011), and this capability is known to be severely impaired in FTLD patients (Hornberger et al., 2012, 2010). Anti-GluA3 hIgGs-treated animals showed a reduced discrimination index 5 min after the acquisition phase (Fig. 2D), suggesting that mice failed or were not interested to recognise the novel object. However, anti-GluA3 administration did not impair recognition memory after 2 hours (Fig. 2E).

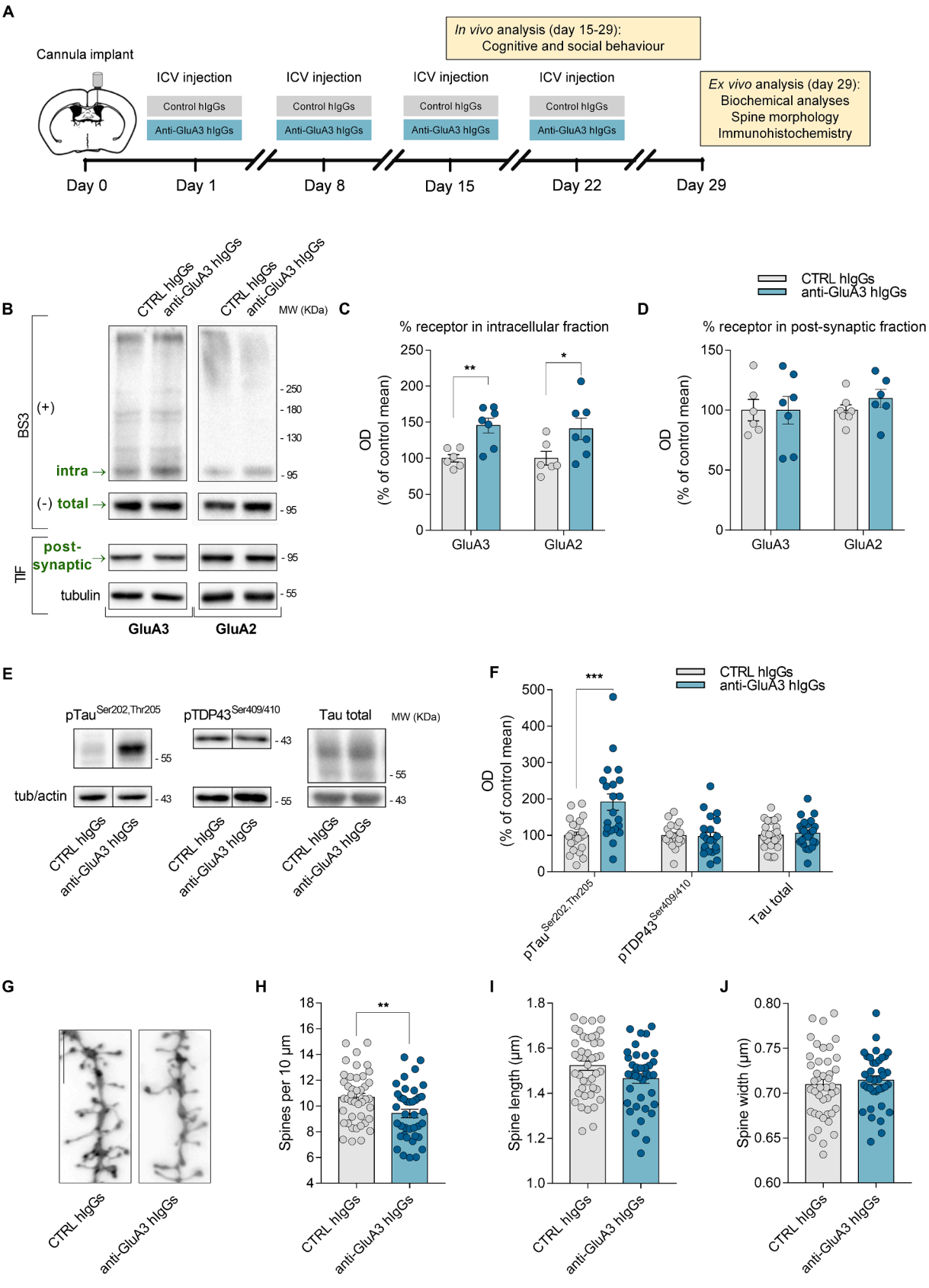

(caption on next page)

Fig. 1. Effects of chronic injection of anti-GluA3 hIgGs on AMPAR surface expression, FTLD-related neuropathological markers, and spine morphology. (**A**) Schematic representation of the experimental timeline. At day 0, mice are implanted with an intracerebroventricular cannula and then injected once a week (at days 1,8,15,22) with purified anti-GluA3 hIgGs or CTRL hIgGs. From day 15 to day 29, mice are tested in different behavioural tasks. At day 29, mice are sacrificed for *ex vivo* analyses on PFC. (**B**) Western blot representative images and bar graph of densitometric quantification of GluA3 and GluA2 in (**C**) intracellular fraction (from BS3 experiment, the blotted values represent the intracellular fraction band normalized on the total amount band) (two-tailed unpaired t-test; GluA3: $t(11) = 3.722$, $p = 0.0034$, $n = 6–7$/group; GluA2: $t(11) = 2.215$, $p = 0.0488$, $n = 6–7$/group) or in (**D**) Triton-insoluble postsynaptic fractions (TIF) obtained from mice PFC at the end of chronic treatment (two-tailed unpaired t-test; GluA3: $t(11) = 0.008576$, $p = 0.9933$, $n = 6–7$/group; GluA2: $t(11) = 1.131$, $p = 0.2823$, $n = 7–6$/group). (**E**) Western blot representative images and (**F**) bar graph of densitometric quantification of p-Tau (Ser202, Thr205, AT8), pTDP43 (Ser409,410) and tau total in Triton-insoluble postsynaptic fraction (TIF) obtained from mice PFC at the end of chronic treatment (two-tailed Mann-Whitney test or two-tailed unpaired t-test; p-Tau: $U = 91$, $p = 0.0004$, $n = 22–21$/group; pTDP43: $t(40) = 0.218$, $p = 0,8285$, $n = 21–21$/group; Tau total: $t(48) = 0.5962$, $p = 0,5538$, $n = 26–24$/group). (**G**) Representative images showing dendrites of adult mice PFC at the end of the chronic treatment with either anti-GluA3 hIgGs and CTRL hIgGs (scale bar = 5μ); bar graphs representing (**H**) protrusion densities (two-tailed unpaired t-test; $t(80) = 2.794$, $p = 0.0065$, $n = 43–39$/group), (**I**) spine length (two-tailed unpaired t-test; $t(80) = 1,931$, $p = 0.0570$, $n = 43–39$/group), and (**J**) spine head width (two-tailed unpaired t-test; $t(78) = 0.6222$, $p = 0.5356$, $n = 43–37$/group). Bar graphs show mean ± s.e.m. In (C), (D), (F), n = number of animals; in (H), (I), (J), n = number of neurons. $^{*}P < 0.05$; $^{**}P < 0.01$; $^{***}P < 0.001$. To apply two-tailed unpaired *t*-test, normal distribution was checked using D'Agostino & Pearson normality test or (when n insufficient) Shapiro-Wilk normality test.

To investigate whether the reduced interest was limited to exploration or could be generalised to other natural stimuli, we assessed the mice's propensity for social stimuli and food via the Affective Discrimination Task and the Free Reward Consumption Task, respectively.

The Affective Discrimination Task measures the ability of mice to discriminate conspecifics based on their affective state. In this task, the mice were presented with two demonstrator mice: one that underwent fear conditioning ('demonstrator fear') or was alternatively subjected to stress ('demonstrator stress') and one that did not receive any manipulation ('demonstrator neutral') (Fig. 2F, G). While CTRL mice preferred to spend more time with the emotionally altered demonstrators, mice injected with anti-GluA3 hIgGs spent a similar amount of time with both demonstrators (Fig. 2H, I).

In the Free Reward Consumption Task, the mice were habituated to a novel cage where they received 50 palatable reward pellets for 2 hours. At the end of the 2 hours, we measured the number of pellets eaten by the mice. We evaluated mice both under the conditions of satiety and after a period of food restriction, and we found that anti-GluA3 hIgGs-treated mice exhibited a reduced interest in food reward consumption compared with CTRL mice under both conditions (Fig. 2J).

Overall, these data indicate that chronic anti-GluA3 hIgGs administration affects locomotor activity in mice, their capability to discriminate a novel object and an emotionally altered conspecific, and their interest in food consumption. Taken together, these results suggest a reduction of interest and preference for novelty following chronic anti-GluA3 hIgGs administration.

3.3. Chronic anti-GluA3 hIgGs administration can trigger hyper-orality or binge-like eating in mice

To further explore the propensity of the mice for food reward, we evaluated their food-seeking behaviour using an operant conditioning task. Mice were presented with two nose-poke holes: an active hole, which delivered one food reward pellet upon nose-poking (fixed ratio = 1), and an inactive hole, which did not produce any effect (Fig. 3A). Under the conditions of food restriction, both groups showed a positive preference index (Fig. 3B), suggesting that they preferred the food-related response; however, anti-GluA3 hIgGs-treated mice exhibited a higher number of food-related responses (Fig. 3D). Moreover, anti-GluA3 hIgGs-treated mice exhibited food-associated responses at shorter time intervals, as indicated by reduced latencies between responses (*Avg. food latency,* Fig. 3C). Analysing the number of food responses as a function of time, we found that the difference in this parameter at the end of the session was entirely attributed to the behaviour of anti-GluA3 hIgGs-treated mice during the first 10 min (Fig. 3E). Similarly, plotting the time as a function of food-related responses, it was clear that anti-GluA3 hIgGs-treated mice required much less time to achieve the same result in terms of food rewards (Fig. 3F). We obtained similar results evaluating mice under conditions of satiety (Fig. S8A, B, C). These results suggest that anti-GluA3 hIgGs-treated mice search for food in a more compulsive way than CTRL mice. We then increased the cost of food-related actions by reinforcing the responses from a fixed ratio of 1 to 4 or 8. Under these conditions, 4 or 8 nose pokes were required to make a food-related response, whereas only 1 nose-poke was necessary for the other response. However, in this case, we did not detect any differences between the two groups (Fig. S8D, E).

A temporal pattern of reward consumption similar to the one obtained in the Food Seeking Task with fixed ratio of 1 was evident in the Sucrose Preference Task. In this task, the mice can choose between water and a solution of water supplemented with 1% sucrose. We observed no differences between the two groups at the end of the task (Figs. 3G; S8F). However, we observed temporal effects during this task: anti-GluA3 hIgGs-treated mice showed an increased preference for the sucrose solution (measured as *sucrose preference* and *sucrose consumption*) compared with the CTRL group in the first 12 hours (Figs. 3G; S8F).

Finally, to determine whether reward-seeking behaviour could have an impact on mouse diet, we weighed mice at the end of chronic treatment (Fig. 3H). Anti-GluA3 hIgGs-treated mice, compared with CTRL mice, had increased weight following the chronic administration. Monitoring mouse weight during treatment, we found that the difference at day 29 was most likely attributed to the eating behaviour of the mice during the final weeks that is when the chronic model of anti-GluA3 hIgGs administration had already been established (Fig. 3I).

These results suggest that chronic anti-GluA3 hIgGs treatment can trigger hyperorality or binge-like eating in mice.

3.4. Behavioural and molecular features in FTLD patients

Previous clinical data from our group suggest that anti-GluA3-Ab+ FTLD patients have marked impairments in glutamatergic neurotransmission (Borroni et al., 2017; Palese et al., 2020). In the present study, we demonstrated that chronic administration of anti-GluA3 hIgGs elicited similar detrimental effects in mice. Moreover, in mice, these defects were paralleled by other specific molecular and behavioural alterations. Therefore, we decided to go back to clinics to investigate whether the anti-GluA3 hIgGs-mediated alterations identified in the preclinical model were also present in GluA3-Ab+ FTLD patients.

With this aim, 260 FTLD patients were enrolled in the present study, of which 86 (33.1%) were GluA3-Ab+ (see Table 1). We observed a significantly higher frequency of bvFTD patients in the GluA3 Ab+ group vs. Ab- group (58.1% vs 42.0%), whereas CBS patients were significantly less frequent (8.1% vs 21.3%). Behavioural symptoms, evaluated with the frontal behaviour inventory and corrected for age and disease duration, showed significant differences between groups regarding poor judgement and impulsivity, personal neglect, hyperorality/food fads, logopenia, aspontaneity, inattention, inflexibility, and apathy (see Table 1). We did not observe significant differences in other behavioural features or in cognitive tests between groups.

One-way ANCOVA, corrected for age and disease duration, indicated significant differences in CSF p-tau$_{181}$ ($p = 0.016$), but not total tau ($p =$

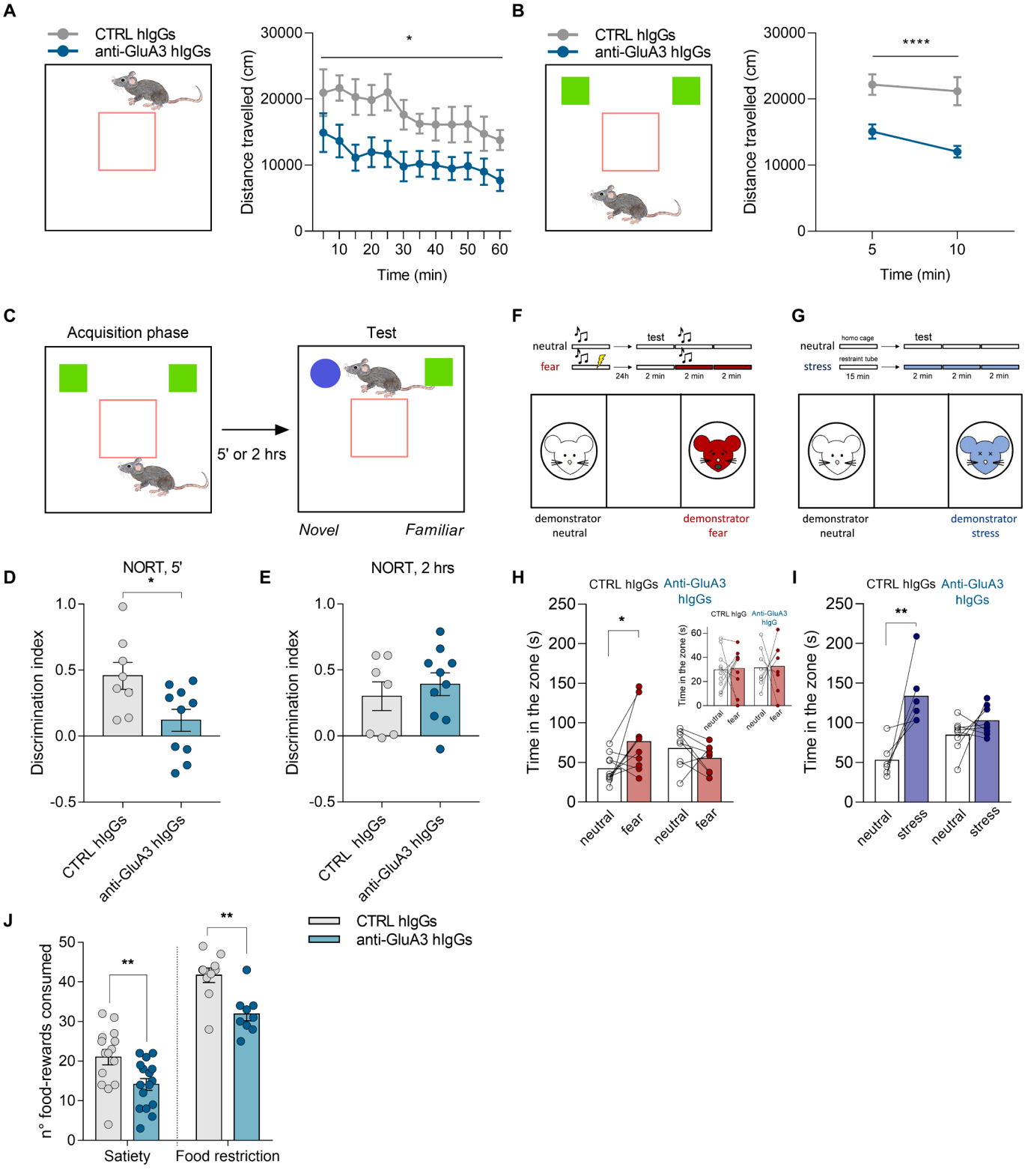

(caption on next page)

Fig. 2. Reduced interest for novelty after chronic anti-GluA3 hIgGs injection. Locomotor activity measured as total distance travelled in the OF arena in (**A**) absence (2way ANOVA; treatment: $F(1,11) = 6.268$, $p = 0.0293$, $n = 6–7$/group) or (**B**) presence of objects (2way ANOVA; treatment: $F(1,28) = 23,62$, $p < 0,0001$, $n = 12–12$/group). (**C**) Novel Oject recognition task (NORT) schematic representation; performance of mice in NORT expressed as discrimination index after (**D**) 5 min (two-tailed unpaired t-test; $t(16) = 2.582$, $p = 0.0201$, $n = 8–10$/group) or (**E**) 2 hrs (two-tailed unpaired t-test; $t(15) = 0.6697$, $p = 0.5132$, $n = 7–10$/group) from the acquisition phase. Schematic representation of Affective Discrimination Task (ADT) with 'neutral' and (**F**) 'fear' or (**G**) 'stress' demonstrators; performance of mice in the ADT expressed as the time spent in the chamber with a neutral demonstrator and in the chamber with (**H**) fear (2way ANOVA; Interaction: $F(1,16) = 6.471$, $p = 0.0217$, $n = 10–8$/group; Bonferroni correction) or (**I**) stress (2way ANOVA; Interaction: $F(1,12) = 6.076$, $p = 0.0298$, $n = 6–8$/group; Bonferroni correction) demonstrator during 4 min after the presentation of the conditioned tone (fear) or during the entire 6 min of test (stress). (**H**) *Inset,* performance of mice in the ADT expressed as the time spent in the chamber with a neutral demonstrator and in the chamber with fear (2way ANOVA; Interaction: $F(1,16) = 4,884e-005$, $p = 0.9945$, $n = 10–8$/group; Bonferroni correction) during the initial 2 min of the test that is before the presentation of the conditioned tone. (**J**) Number of palatable pellets of food consumed in the free reward consumption task by mice in both a condition of satiety (two-tailed unpaired t-test; $t(29) = 2.838$, $p = 0.0082$, $n = 15–16$/group) and after a period of food restriction (Mann-Whitney test; $U = 12$, $p = 0.0053$, $n = 10–9$/group). Bar graphs show mean ± s.e.m. n = number of animals. $^{*}P < 0.05$; $^{**}P < 0.01$; $^{****}<0.0001$. To apply two-tailed unpaired *t*-test, normal distribution was checked using D'Agostino & Pearson normality test or (when n insufficient) Shapiro-Wilk normality test.

0.278) or amyloid-$\beta_{1\text{-}42}$ (p = 0.177) (see Table 1). Notably, the p-tau results were in parallel with what we identified in the pre-clinical model, where, in the post-synaptic compartment, chronic anti-GluA3 hIgGs administration triggered the accumulation of p-tau without affecting total tau levels.

Overall, these data indicate that anti-GluA3-hIgGs-treated mice show high overlap with the disease symptomatology of FTLD patients positive for anti-GluA3 Abs. The anti-GluA3-Ab+ patients exhibited accentuated hyperorality, inattention, and apathy, which are the main behavioural traits that characterised our pre-clinical model of chronic anti-GluA3 hIgGs administration (Figs. 2, 3). Furthermore, this correlation with clinical data indicates the high face validity of our pre-clinical model, which makes it a valuable tool for gaining insights into human pathology and testing new therapeutic personalised medicine approaches.

3.5. The administration of PAM s 47445 rescued anti-GluA3 hIgGs-mediated detrimental effects

Chronic administration of anti-GluA3 hIgGs led to a significant reduction in the surface retention of GluA3/GluA2 AMPARs (Fig. 1C). Considering these results and the reduction of glutamatergic transmission previously observed in anti-GluA3-Ab+ patients by neurophysiological techniques (Palese et al., 2020), we hypothesised that the stimulation of AMPARs still available at the post-synaptic membrane could counteract the detrimental effects of anti-GluA3 hIgGs on the glutamatergic system. To test this hypothesis, we treated mice with a well-validated AMPAR PAM, namely S 47445 (tulrampator, CX-1632) (Bretin et al., 2017). This molecule produces a robust increase in AMPAR activation in different pre-clinical *in vivo* studies (Bretin et al., 2017; Giralt et al., 2017) and has previously been assessed in a clinical trial (Clinicaltrials.gov identifier NCT number: NCT02805439). We administered S 47445 daily from day 15 to day 29 through intraperitoneal injection (Fig. 4A). Indeed, the behavioural results suggested that the detrimental effects mediated by chronic anti-GluA3 hIgGs administration were present from at least day 15.

S 47445 administration fully rescued anti-GluA3 hIgGs-mediated accumulation of p-tau in the post-synaptic compartment (Fig. 4B, C). In addition, we observed total recovery of spine density in the anti-GluA3 hIgGs-treated animals that received daily administration of S 47445 (Fig. 4D, E). Therefore, the chronic stimulation of AMPAR-mediated glutamatergic neurotransmission by S 47445 administration was sufficient to rescue the molecular and morphological detrimental effects induced by anti-GluA3 hIgGs. Importantly, this event was paralleled by recovery of anti-GluA3 hIgGs-mediated behavioural defects. Mice treated with S 47445 recovered their interest in novelty both in terms of exploration (Fig. 5A, C, D) and food consumption (Fig. 5B). Furthermore, we detected partial recovery of binge-like eating behaviour assessed in operant boxes (Figs. 5E–J; S9A–C). As reported in Fig. 5I, J, the administration of S 47445 to anti-GluA3 hIgGs-treated mice defined a new group of animals with a food-seeking behaviour (expressed as the number of food-related responses) that was exactly in the middle between the CTRL mice and anti-GluA3 hIgGs-treated mice. Overall, both *ex vivo* and behavioural data indicated that chronic S 47445 administration counteracted anti-GluA3 hIgGs-mediated detrimental effects.

4. Discussion

Recently, autoantibodies directed against the GluA3 subunit of AMPARs have been identified in 20%–25% FTLD patients (Borroni et al., 2017; Palese et al., 2020). The present study allowed us to elucidate the specific contribution of anti-GluA3 hIgGs antibodies to the central nervous system symptoms and identify a new putative approach for personalised medicine that may be suitable for anti-GluA3-Ab+ patients.

As previously demonstrated (Haselmann et al., 2018; Hughes et al., 2010; Lai et al., 2009; Maudes et al., 2022; Mikasova et al., 2012; Peng et al., 2015), pathogenic IgG antibodies targeting extracellular epitopes of membrane receptors often promote the endocytosis of the receptor. In the present study, we demonstrated that chronic anti-GluA3 hIgGs administration in mice mediated a selective increase in the intracellular levels of GluA3-containing AMPAR and a consequent decrease in their surface retention. As we did not detect any differences in GluA3-containing AMPAR levels in the post-synaptic fraction, we hypothesised that anti-GluA3 hIgGs induced an endocytic process of GluA3-containing AMPARs within the dendritic spine compartment.

We found that chronic anti-GluA3 hIgGs administration in mice led to selective accumulation of the p-tau in the post-synaptic compartment. Remarkably, we also detected an increase in the level of p-tau in the CSF of GluA3-Ab+ FTLD patients compared with FTLD patients not carrying the autoantibody. Even if most of the published study mainly indicated CSF p-tau181 levels in FTD similar to controls (Constantinides et al., 2023), other studies showed the presence of higher levels in FTD patients as compared to controls (Grossman et al., 2005). It remains to be clarified whether the increase of p-tau181 levels in FTLD was related to a specific neuropathological hallmark of the disease or to a co-occurrence of AD pathology. However, our FTLD patients positive for anti-GluA3 antibody and with increased p-tau181 levels presented CSF total tau and Abeta42 within normal range, excluding an AD-like pattern profile.

A large body of literature suggests that a variety of toxic stimuli can trigger aberrant tau phosphorylation. In its hyperphosphorylated form, tau is more prone to aggregate to form the toxic inclusions that characterise tauopathies (Alonso and Cohen, 2018; Bodea et al., 2016). However, recent studies have indicated that tau hyperphosphorylation also promotes its migration into the postsynaptic compartment (Italia et al., 2022). In this compartment, p-tau negatively affects synapse functionality as it interferes with ionotropic glutamate receptors: several studies reported a reduction in the activity and in the synaptic expression of AMPAR and NMDAR in the presence of tau mislocalisation and hyperphosphorylation (Alfaro-Ruiz et al., 2022; Hoover et al., 2010; Li et al., 2019; Miller et al., 2014; Prikas et al., 2022; Regan et al., 2021; Teravskis et al., 2021). Other studies also suggested that acting on glutamatergic signalling, and specifically potentiating AMPAR, prevents

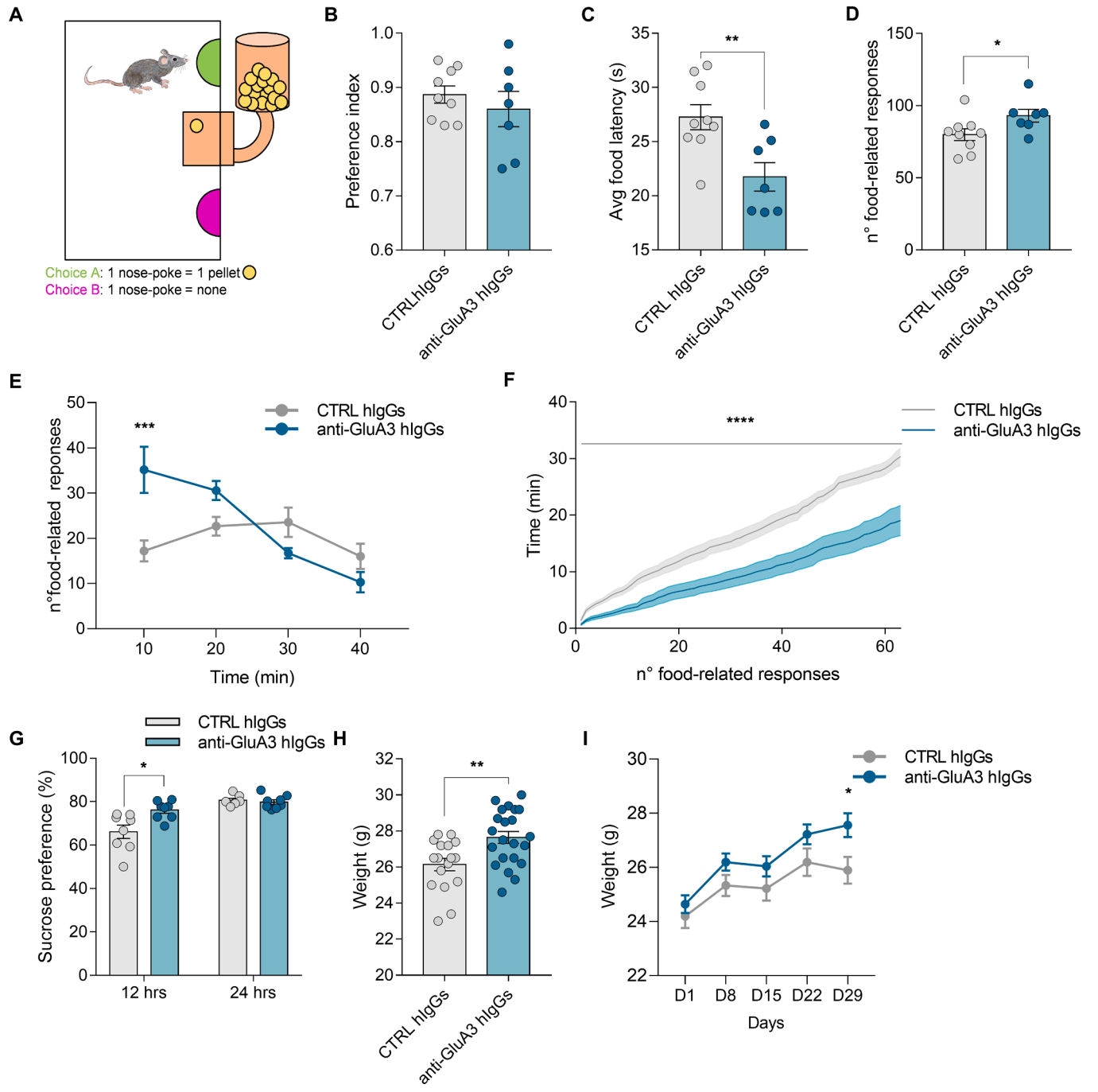

Fig. 3. Binge-like eating and impulsivity after chronic anti-GluA3 hIgGs injection. (**A**) Schematic representation of the Food Seeking task in the operant boxes: over a period of 40′, mice can choose between a nose-poke that delivers one palatable pellet of food (choice A) and a nose-poke that does not produce any effect (choice B); mice performance in the food seeking task expressed as (**B**) preference index (two-tailed unpaired t-test; $t(14) = 0.7939$, $p = 0.4405$, $n = 9$–7/group), (**C**) average of time between one food-related response and the subsequent one (*i.e.*, *avg food latency*) (two-tailed unpaired t-test; $t(14) = 3.146$, $p = 0.0072$, $n = 9$–7/group) and (**D**) number of food-related responses (choice A) (two-tailed unpaired t-test; $t(14) = 2.169$, $p = 0.0478$, $n = 9$–7/group); in (**E-F**) the number of food-related responses within the session in operant boxes is reported: in (**E**), the number of food-related responses is reported as a function of time (2way ANOVA; interaction: $F(3,42) = 7.561$, $p = 0.0004$, $n = 9$–7/group; Bonferroni correction) whereas in (**F**) is highlighted the time required to perform a certain number of food-related responses (2way ANOVA; interaction: $F(62,868) = 7.925$, $p < 0.0001$, $n = 9$–7/group). In (**A-F**) the task was performed by mice that underwent food restriction. (**G**) Mice performance in the Sucrose Preference Task expressed as Sucrose preference in percentage (two-tailed unpaired t-test; 12 hrs: $t(14) = 2.907$, $p = 0.0115$, $n = 8$–8/group; 24 h: $t(13) = 0.5992$, $p = 0.5594$, $n = 7$–8/group). Mice weight (**H**) at the end of the chronic treatment (D29) (two-tailed unpaired t-test; $t(37) = 3.125$, $p = 0.0034$, $n = 17$–22/group) and (**I**) monitored once a week (2way ANOVA; treatment: $F(1,23) = 4.54$, $p = 0.0440$, $n = 11$–14/group; Bonferroni correction). Bar graphs show mean ± s.e.m. n = number of animals. $^{*}P < 0.05$; $^{**}P < 0.01$; $^{***}P < 0.001$; $^{****}P < 0.0001$. To apply two-tailed unpaired *t*-test, normal distribution was checked using D'Agostino & Pearson normality test or (when n insufficient) Shapiro-Wilk normality test.

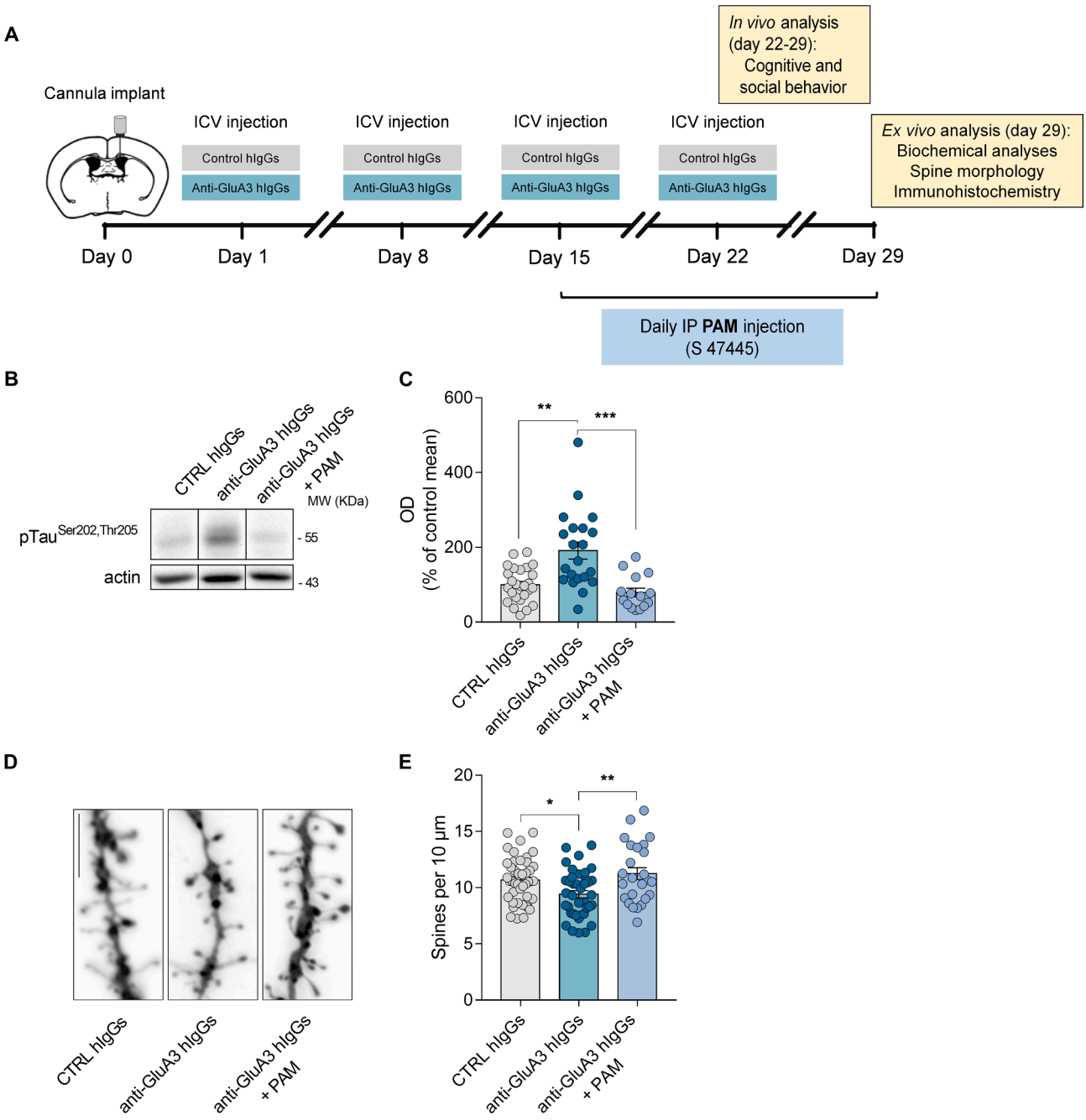

Fig. 4. PAM administration totally rescued anti-GluA3-hIgGs-mediated detrimental effects in terms of p-tau accumulation and loss of dendritic spines. (**A**) Scheme representing the timeline of rescue strategy administration to chronic animal model: mice receive daily intraperitoneal (IP) injection of PAM S 47445 from day 15 to day 29. (**B**) Western blot representative images and (**C**) bar graph of densitometric quantification of p-Tau (Ser202, Thr205, AT8) in TIF obtained from mice PFC at the end of chronic treatment with CTRL hIgGs and anti-GluA3 hIgGs ± PAM (Kruskal-Wallis; $p = 0.0001$, $n = 26–21-15$/group; Dunn's correction). (**D**) Representative images showing dendrites of adult mice PFC at the end of the chronic treatment with CTRL hIgGs or anti-GluA3 hIgGs ± PAM and bar graphs representing (**E**) protrusion densities (ordinary one-way ANOVA; treatment: $F(2.104) = 6.034$, $p = 0.0033$, $n = 43–39-25$/group; Tukey correction). Bar graphs show mean ± s.e.m. In (**C**), n = number of animals; in (**E**), n = number of neurons. $^{*}P < 0.05$; $^{**}P < 0.01$; $^{***}P < 0.001$. To apply one-way ANOVA, normal distribution was checked using D'Agostino & Pearson normality test.

tau-mediated toxic synaptic effects (Monteiro-Fernandes et al., 2021), suggesting that the toxic crosstalk between AMPAR and tau could also be the explained the other way around.

Along with molecular and morphological alterations, anti-GluA3 hIgGs induce a peculiar behavioural signature in mice characterised by a reduction in interest for novelty in addition to binge-like eating and impulsivity. We assessed the reduction in interest for novelty through different stimuli. In the tasks, mice were presented with a series of stimuli entailing a progressive increase in the required cognitive load. Anti-GluA3 hIgGs-treated mice failed to discriminate between salient stimuli involving newly presented objects, emotionally altered conspecifics, and palatable pellets of food. Therefore, these features could be interpreted as a reduction of interest or inattention for novelty rather than a deficit in recognition, which is consistent with the reduced interest for exploration in different environmental conditions.

We found contrasting behavioural responses when food rewards were presented to home caged mice or following operant conditioning. However, it must be highlighted that these two conditions entailed

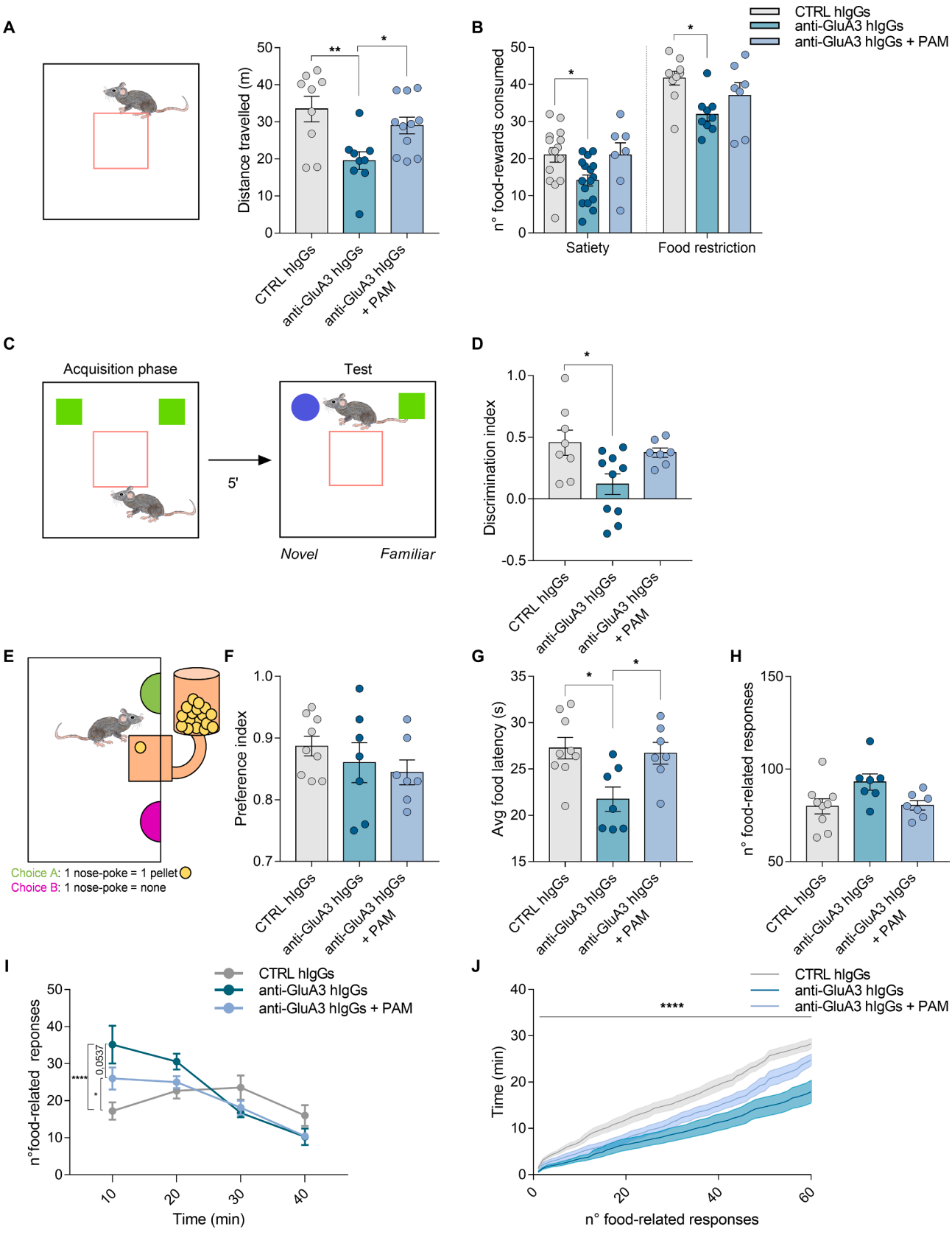

(caption on next page)

Fig. 5. PAM administration partially or totally rescued anti-GluA3 hIgGs-mediated behavioural effects. (**A**) Locomotor activity measured as the total distance travelled in the OF arena in the first 10 min of exploration (ordinary one-way ANOVA; treatment: $F(2,26) = 6.537$, $p = 0.0050$, $n = 9$–9-11/group; Tukey correction). (**B**) Number of palatable pellets of food consumed in the Free Reward Consumption task by mice in a condition of satiety (ordinary one-way ANOVA; treatment: $F(2,35) = 4.344$, $p = 0.0206$, $n = 15$–16-7/group; Tukey correction) or after a period of food restriction (ordinary one-way ANOVA; treatment: $F(2,23) = 5.126$, $p = 0.0144$, $n = 10$–9–7/group; Tukey correction). (**C**) NORT schematic representation; performance of mice in NORT expressed as discrimination index after (**D**) 5 min from the acquisition phase (ordinary one-way ANOVA; treatment: $F(2,22) = 4.856$, $p = 0.0179$, $n = 8$–10-7/group; Tukey correction). (**E**) Schematic representation of the food seeking task; mice performance in the food seeking task expressed as (**F**) preference index (ordinary one-way ANOVA; treatment: $F(2,20) = 0.9339$, $p = 0.4095$, $n = 9$–7-7/group; Tukey correction), (**G**) average of time between one food-related response and the subsequent one (*i.e.*, *avg food latency*) (ordinary one-way ANOVA; treatment: $F(2,20) = 5.992$, $p = 0.0091$, $n = 9$–7-7/group; Tukey correction) and (**H**) number of food-related responses (choice A) (ordinary one-way ANOVA; treatment: $F(2,20) = 3.535$, $p = 0.0485$, $n = 9$–7-7/group; Tukey correction); in (**I-J**) number of food-related responses during the session in operant boxes are reported ((**I**): 2way ANOVA; interaction: $F(6,60) = 4.668$, $p = 0{,}0006$, $n = 9$–7-7/group; Tukey correction; (**J**): 2way ANOVA; interaction: $F(124,1240) = 5.067$, $p < 0{,}0001$, $n = 9$–7-7/group)). In (**F-J**) the task was performed by mice that underwent food restriction. Bar graphs show mean ± s.e.m. n = number of animals. $^{*}P < 0.05$; $^{**}P < 0.01$; $^{****}P < 0.0001$. To apply one-way ANOVA, normal distribution was checked using D'Agostino & Pearson normality test or (when n insufficient) Shapiro-Wilk normality test.

rather different cognitive processing; under the first condition, mice had free access to palatable pellets of food, whereas, in the second, they actively sought out food. The latter scenario triggered binge-eating-like behaviour and impulsivity in anti-GluA3 hIgGs-treated mice. A similar impulsive behaviour was observed in the sucrose preference test. However, we did not observe any differences when we increased the fixed ratio schedule. As previously described in the literature for a murine model of obesity (Bickel et al., 2021; Matikainen-Ankney et al., 2022), this may be explained by the fact that anti-GluA3-treated mice exhibited increased intolerance towards delayed rewards (consequently, it could be a matter of time rather than effort). Overall, our results suggest that anti-GluA3 hIgGs can affect the reward system in general by negatively influencing mice's attitudes towards natural stimuli/rewards.

In line with these findings, previous studies mainly performed in GRIA3 KO mice suggested a role of GluA3 in the modulation of social behaviour (Adamczyk et al., 2012; Li et al., 2023) in the absence of gross behavioural abnormalities (Adamczyk et al., 2012; Humeau et al., 2007; Sanchis-Segura et al., 2006). In addition, mutations, and polymorphisms in the *GRIA3* gene have been associated with alterations in sociability in humans and the appearance of a more aggressive phenotype (Peng et al., 2022). Overall, these data further support the idea that a reduction in GluA3 activity could contribute to the appearance of behavioural abnormalities.

Anti-GluA3-Ab+ FTLD patients exhibited significant differences in some behavioural traits, such as poor judgement and impulsivity, hyperorality/food fads, inattention, and apathy. These findings were consistent regardless of disease severity, suggesting that the presence of anti-GluA3 antibodies might specifically influence certain behavioural outcomes rather than represent a universally aggressive form of FTLD. The higher association between GluA3-Ab+ and bvFTD may be attributed to the specific effects of GluA3 on neural circuits in the prefrontal and anterior temporal regions, where AMPA receptor disruptions could lead to behavioural symptoms. Alternatively, this association might be due to the role of GluA3 in modulating specific behaviours: in this light, the antibody-mediated impairment in GluA3 activity potentially exacerbates behavioural symptoms. Because the behavioural traits detected in anti-GluA3-Ab+ patients reflect those identified in our pre-clinical model, we concluded that anti-GluA3 hIgGs-treated mice exhibited a high degree of overlap with the disease symptomatology of these patients. In our pre-clinical model, the presence of anti-GluA3 hIgGs alone induced the appearance of signs and symptoms that resembled the ones exhibited by the patients; this correspondence suggests a link of causation between anti-GluA3 hIgGs positivity and the appearance of a specific symptomatology. In addition, it indicates the high face validity of our model, making it a valuable tool not only for gaining insights into human pathophysiology, but also as a tool to evaluate new pharmacological approaches of personalised medicine for anti-GluA3-Ab+ patients.

Finally, of primary relevance, we used our model to evaluate the efficacy of a well-validated AMPAR PAM (S 47445) whose safety was previously approved in a clinical trial (*Clinicaltrials.gov, identifier NCT number: NCT02805439*) and whose efficacy was already validated in different pre-clinical models (Bretin et al., 2017; Calabrese et al., 2017; Mendez-David et al., 2017; Morley-Fletcher et al., 2018). The stimulation of the remaining available AMPAR at the post-synaptic membrane with S 47445 counteracted almost all the deficits induced by anti-GluA3 hIgGs. This result represents a proof of concept that the defects in glutamatergic neurotransmission mediated by anti-GluA3 hIgGs are at the root of the observed molecular and behavioural abnormalities. Moreover, the observed efficacy of S 47445 in our pre-clinical model can pave the way for further studies aimed at investigating the putative clinical use of this class of compounds for precision medicine therapy in GluA3-Ab+ patients. The partial rescue that we observed in some behavioural traits could be due to the dosage of 3 mg/kg used in the present study instead of the 10 mg/kg described in some pre-clinical studies (Mendez-David et al., 2017; Pilar-Cuellar et al., 2019) and due to the timing. The *ex-vivo* analyses were all performed after 15 days of daily PAM administration (*i.e.*, on day 29); the behavioural tasks were performed from day 22 to day 29 on mice that had been treated with PAM for fewer days.

In conclusion, our study clarified the contribution of anti-GluA3 autoantibodies to central nervous system symptoms and pathology and identified a specific subgroup of FTLD patients with distinct clinical features. Our findings will be instrumental in the development of a therapeutic personalised medicine strategy for patients positive for anti-GluA3.

However, the research we have carried out thus far does not address some relevant issues. From the pre-clinical point of view, it would be of interest to evaluate the circuit mechanisms through which anti-GluA3 hIgGs support the observed behavioural abnormalities. Clinically, additional studies on a larger cohort of patients are needed to better understand the mechanisms that support the appearance of the autoantibodies directed against GluA3 subunit. In addition, if on the one hand we demonstrated that the immunoglobulins isolated by affinity purification from a pool of human sera bound native GluA3 subunit in fixed or unfixed live cells, on the other we did not do the same at single sera level. Accordingly, further investigation should be performed prior to the potential adoption of anti-GluA3 hIgGs-based screening as a routine clinical tool and, consequently, its future use for personalized therapies.

5. Source of fundings

This work was supported by grants from:

- Ministero della Salute RF-2019–12369272 to MDL and AP.
- Cariplo Foundation 2021–1516 to FG and AB.
- Sigrid Jusélius Foundation to AH.
- Ministero dell'Istruzione, dell'Universita' e della Ricerca (MIUR) - PRIN (Bando 2022, Prot. 2022YY85P5 to FG, BB, CS).

CRediT authorship contribution statement

Maria Italia: Writing – original draft, Methodology, Investigation, Data curation, Conceptualization. **Michela Salvadè:** Methodology, Investigation, Formal analysis. **Filippo La Greca:** Methodology, Formal analysis. **Elisa Zianni:** Methodology, Formal analysis. **Silvia Pelucchi:** Investigation, Formal analysis, Conceptualization. **Alessio Spinola:** Investigation. **Elena Ferrari:** Investigation. **Silvana Archetti:** Resources, Methodology, Investigation. **Antonella Alberici:** Resources, Investigation. **Alberto Benussi:** Writing – review & editing, Resources, Funding acquisition, Conceptualization. **Eino Solje:** Writing – review & editing, Resources. **Annakaisa Haapasalo:** Writing – review & editing, Resources, Funding acquisition. **Dorit Hoffmann:** Writing – review & editing, Resources. **Kasper Katisko:** Writing – review & editing, Resources. **Johanna Krüger:** Writing – review & editing, Resources. **Roberta Facchinetti:** Investigation, Formal analysis. **Caterina Scuderi:** Writing – review & editing, Methodology, Funding acquisition, Conceptualization. **Alessandro Padovani:** Writing – review & editing, Resources, Conceptualization. **Monica DiLuca:** Writing – review & editing, Funding acquisition, Conceptualization. **Diego Scheggia:** Writing – review & editing, Writing – original draft, Methodology, Conceptualization. **Barbara Borroni:** Writing – review & editing, Writing – original draft, Resources, Funding acquisition, Conceptualization. **Fabrizio Gardoni:** Writing – review & editing, Writing – original draft, Supervision, Funding acquisition, Conceptualization.

Declaration of Competing Interest

The authors declare that they have no known competing financial interests or personal relationships that could have appeared to influence the work reported in this paper.

Data availability

Data will be made available on request.

Appendix A. Supplementary data

Supplementary data to this article can be found online at https://doi.org/10.1016/j.bbi.2024.03.018.

References

Adamczyk, A., Mejias, R., Takamiya, K., Yocum, J., Krasnova, I.N., Calderon, J., Cadet, J. L., Huganir, R.L., Pletnikov, M.V., Wang, T., 2012. GluA3-deficiency in mice is associated with increased social and aggressive behavior and elevated dopamine in striatum. Behav. Brain Res. 229, 265–272. https://doi.org/10.1016/j.bbr.2012.01.007.

Alfaro-Ruiz, R., Aguado, C., Martín-Belmonte, A., Moreno-Martínez, A.E., Merchán-Rubira, J., Hernández, F., Ávila, J., Fukazawa, Y., Luján, R., 2022. Alteration in the synaptic and Extrasynaptic organization of AMPA receptors in the hippocampus of P301S tau transgenic mice. Int. J. Mol. Sci. 23, 13527. https://doi.org/10.3390/ijms232113527.

Alonso, A.D., Cohen, L.S., 2018. Our tau Tales from Normal to pathological behavior. J. Alzheimers Dis. JAD 64, S507–S516. https://doi.org/10.3233/JAD-179906.

Amodeo, G., Verduci, B., Sartori, P., Procacci, P., Conte, V., Balboni, G., Sacerdote, P., Franchi, S., 2021. The antagonism of the prokineticin system Counteracts bortezomib induced side effects: focus on mood alterations. Int. J. Mol. Sci. 22, 10256. https://doi.org/10.3390/ijms221910256.

Armstrong, M.J., Litvan, I., Lang, A.E., Bak, T.H., Bhatia, K.P., Borroni, B., Boxer, A.L., Dickson, D.W., Grossman, M., Hallett, M., Josephs, K.A., Kertesz, A., Lee, S.E., Miller, B.L., Reich, S.G., Riley, D.E., Tolosa, E., Tröster, A.I., Vidailhet, M., Weiner, W.J., 2013. Criteria for the diagnosis of corticobasal degeneration. Neurology 80, 496–503. https://doi.org/10.1212/WNL.0b013e31827f0fd1.

Arshad, F., Varghese, F., Paplikar, A., Gangadhar, Y., Ramakrishnan, S., Chaudhuri, J.R., Mahadevan, A., Alladi, S., 2021. Role of autoantibodies in neurodegenerative dementia: an Emerging association. Dement. Geriatr. Cogn. Disord. 50, 153–160. https://doi.org/10.1159/000517238.

Barker, G.R.I., Warburton, E.C., 2011. When is the hippocampus involved in recognition memory? J. Neurosci. off. J. Soc. Neurosci. 31, 10721–10731. https://doi.org/10.1523/JNEUROSCI.6413-10.2011.

Benjamini, Y., Hochberg, Y., 1995. Controlling the false discovery rate: a Practical and powerful approach to multiple testing. J. r. Stat. Soc. Ser. B Methodol. 57, 289–300. https://doi.org/10.1111/j.2517-6161.1995.tb02031.x.

Benussi, A., Gazzina, S., Premi, E., Cosseddu, M., Archetti, S., Dell'Era, V., Cantoni, V., Cotelli, M.S., Alberici, A., Micheli, A., Benussi, L., Ghidoni, R., Padovani, A., Borroni, B., 2019. Clinical and biomarker changes in presymptomatic genetic frontotemporal dementia. Neurobiol. Aging 76, 133–140. https://doi.org/10.1016/j.neurobiolaging.2018.12.018.

Bickel, W.K., Freitas-Lemos, R., Tomlinson, D.C., Craft, W.H., Keith, D.R., Athamneh, L. N., Basso, J.C., Epstein, L.H., 2021. Temporal discounting as a candidate behavioral marker of obesity. Neurosci. Biobehav. Rev. 129, 307–329. https://doi.org/10.1016/j.neubiorev.2021.07.035.

Bodea, L.-G., Eckert, A., Ittner, L.M., Piguet, O., Götz, J., 2016. Tau physiology and pathomechanisms in frontotemporal lobar degeneration. J. Neurochem. 138 (Suppl 1), 71–94. https://doi.org/10.1111/jnc.13600.

Borroni, B., Benussi, A., Archetti, S., Galimberti, D., Parnetti, L., Nacmias, B., Sorbi, S., Scarpini, E., Padovani, A., 2015. Csf p-tau181/tau ratio as biomarker for TDP pathology in frontotemporal dementia. Amyotroph. Lateral Scler. Front. Degener. 16, 86–91. https://doi.org/10.3109/21678421.2014.971812.

Borroni, B., Stanic, J., Verpelli, C., Mellone, M., Bonomi, E., Alberici, A., Bernasconi, P., Culotta, L., Zianni, E., Archetti, S., Manes, M., Gazzina, S., Ghidoni, R., Benussi, L., Stuani, C., Di Luca, M., Sala, C., Buratti, E., Padovani, A., Gardoni, F., 2017. Anti-AMPA GluA3 antibodies in frontotemporal dementia: a new molecular target. Sci. Rep. 7, 6723. https://doi.org/10.1038/s41598-017-06117-y.

Bretin, S., Louis, C., Seguin, L., Wagner, S., Thomas, J.-Y., Challal, S., Rogez, N., Albinet, K., Iop, F., Villain, N., Bertrand, S., Krazem, A., Bérachochéa, D., Billiald, S., Tordjman, C., Cordi, A., Bertrand, D., Lestage, P., Danober, L., 2017. Pharmacological characterisation of S 47445, a novel positive allosteric modulator of AMPA receptors. PloS One 12, e0184429. https://doi.org/10.1371/journal.pone.0184429.

Calabrese, F., Savino, E., Mocaer, E., Bretin, S., Racagni, G., Riva, M.A., 2017. Upregulation of neurotrophins by S 47445, a novel positive allosteric modulator of AMPA receptors in aged rats. Pharmacol. Res. 121, 59–69. https://doi.org/10.1016/j.phrs.2017.04.019.

Constantinides, V.C., Paraskevas, G.P., Boufidou, F., Bourbouli, M., Pyrgelis, E.-S., Stefanis, L., Kapaki, E., 2023. CSF Aβ42 and Aβ42/Aβ40 ratio in Alzheimer's disease and frontotemporal dementias. Diagn. Basel Switz. 13, 783. https://doi.org/10.3390/diagnostics13040783.

Cosseddu, M., Benussi, A., Gazzina, S., Turrone, R., Archetti, S., Bonomi, E., Biasiotto, G., Zanella, I., Ferrari, R., Cotelli, M.S., Alberici, A., Padovani, A., Borroni, B., 2018. Mendelian forms of disease and age at onset affect survival in frontotemporal dementia. Amyotroph. Lateral Scler. Front. Degener. 19, 87–92. https://doi.org/10.1080/21678421.2017.1384020.

Cosseddu, M., Benussi, A., Gazzina, S., Alberici, A., Dell'Era, V., Manes, M., Cristillo, V., Borroni, B., Padovani, A., 2020. Progression of behavioural disturbances in frontotemporal dementia: a longitudinal observational study. Eur. J. Neurol. 27, 265–272. https://doi.org/10.1111/ene.14071.

Day, C., Silva, J.-P., Munro, R., Baker, T.S., Wolff, C., Bithell, A., Stephens, G.J., 2023. Anti-AMPA receptor autoantibodies reduce excitatory currents in rat hippocampal neurons. Pharm. Basel Switz. 16, 77. https://doi.org/10.3390/ph16010077.

Duong, S.L., Prüss, H., 2023. Molecular disease mechanisms of human antineuronal monoclonal autoantibodies. Trends Mol. Med. 29, 20–34. https://doi.org/10.1016/j.molmed.2022.09.011.

Ferrari, E., Scheggia, D., Zianni, E., Italia, M., Brumana, M., Palazzolo, L., Parravicini, C., Pilotto, A., Padovani, A., Marcello, E., Eberini, I., Calabresi, P., Diluca, M., Gardoni, F., 2022. Rabphilin-3A as a novel target to reverse α-synuclein-induced synaptic loss in Parkinson's disease. Pharmacol. Res. 183, 106375 https://doi.org/10.1016/j.phrs.2022.106375.

Ferretti, V., Maltese, F., Contarini, G., Nigro, M., Bonavia, A., Huang, H., Gigliucci, V., Morelli, G., Scheggia, D., Managò, F., Castellani, G., Lefevre, A., Cancedda, L., Chini, B., Grinevich, V., Papaleo, F., 2019. Oxytocin signaling in the central amygdala modulates emotion discrimination in mice. Curr. Biol. CB 29, 1938–1953.e6. https://doi.org/10.1016/j.cub.2019.04.070.

Gardoni, F., Saraceno, C., Malinverno, M., Marcello, E., Verpelli, C., Sala, C., Di Luca, M., 2012. The neuropeptide PACAP38 induces dendritic spine remodeling through ADAM10-N-cadherin signaling pathway. J. Cell Sci. 125, 1401–1406. https://doi.org/10.1242/jcs.097576.

Gardoni, F., Stanic, J., Scheggia, D., Benussi, A., Borroni, B., Di Luca, M., 2021. NMDA and AMPA receptor autoantibodies in brain Disorders: from Molecular mechanisms to clinical features. Cells 10, 77. https://doi.org/10.3390/cells10010077.

Giralt, A., Gómez-Climent, M.Á., Alcalá, R., Bretin, S., Bertrand, D., María Delgado-García, J., Pérez-Navarro, E., Alberch, J., Gruart, A., 2017. The AMPA receptor positive allosteric modulator S 47445 rescues in vivo CA3-CA1 long-term potentiation and structural synaptic changes in old mice. Neuropharmacology 123, 395–409. https://doi.org/10.1016/j.neuropharm.2017.06.009.

Gorno-Tempini, M.L., Hillis, A.E., Weintraub, S., Kertesz, A., Mendez, M., Cappa, S.F., Ogar, J.M., Rohrer, J.D., Black, S., Boeve, B.F., Manes, F., Dronkers, N.F., Vandenberghe, R., Rascovsky, K., Patterson, K., Miller, B.L., Knopman, D.S., Hodges, J.R., Mesulam, M.M., Grossman, M., 2011. Classification of primary progressive aphasia and its variants. Neurology 76, 1006–1014. https://doi.org/10.1212/WNL.0b013e31821103e6.

Grossman, M., Farmer, J., Leight, S., Work, M., Moore, P., Van Deerlin, V., Pratico, D., Clark, C.M., Coslett, H.B., Chatterjee, A., Gee, J., Trojanowski, J.Q., Lee, V.-M.-Y., 2005. Cerebrospinal fluid profile in frontotemporal dementia and Alzheimer's disease. Ann. Neurol. 57, 721–729. https://doi.org/10.1002/ana.20477.

Hansen, N., 2021. Current nosology of neural autoantibody-associated dementia. Front. Aging Neurosci. 13, 711195 https://doi.org/10.3389/fnagi.2021.711195.
Hansen, N., Stöcker, W., Wiltfang, J., Bartels, C., Rentzsch, K., Bouter, C., 2021. Case report: semantic Variant of Primary progressive aphasia associated with anti-glial Fibrillary acid protein autoantibodies. Front. Immunol. 12, 760021 https://doi.org/10.3389/fimmu.2021.760021.
Harris, K.M., Jensen, F.E., Tsao, B., 1992. Three-dimensional structure of dendritic spines and synapses in rat hippocampus (CA1) at postnatal day 15 and adult ages: implications for the maturation of synaptic physiology and long-term potentiation. J. Neurosci. off. J. Soc. Neurosci. 12, 2685–2705. https://doi.org/10.1523/JNEUROSCI.12-07-02685.1992.
Haselmann, H., Mannara, F., Werner, C., Planagumà, J., Miguez-Cabello, F., Schmidl, L., Grünewald, B., Petit-Pedrol, M., Kirmse, K., Classen, J., Demir, F., Klöcker, N., Soto, D., Doose, S., Dalmau, J., Hallermann, S., Geis, C., 2018. Human autoantibodies against the AMPA receptor subunit GluA2 induce receptor reorganization and memory dysfunction. Neuron 100, 91–105.e9. https://doi.org/10.1016/j.neuron.2018.07.048.
Höglinger, G.U., Respondek, G., Stamelou, M., Kurz, C., Josephs, K.A., Lang, A.E., Mollenhauer, B., Müller, U., Nilsson, C., Whitwell, J.L., Arzberger, T., Englund, E., Gelpi, E., Giese, A., Irwin, D.J., Meissner, W.G., Pantelyat, A., Rajput, A., van Swieten, J.C., Troakes, C., Antonini, A., Bhatia, K.P., Bordelon, Y., Compta, Y., Corvol, J.-C., Colosimo, C., Dickson, D.W., Dodel, R., Ferguson, L., Grossman, M., Kassubek, J., Krismer, F., Levin, J., Lorenzl, S., Morris, H.R., Nestor, P., Oertel, W.H., Poewe, W., Rabinovici, G., Rowe, J.B., Schellenberg, G.D., Seppi, K., van Eimeren, T., Wenning, G.K., Boxer, A.L., Golbe, L.I., Litvan, I., Movement Disorder Society-endorsed PSP Study Group, 2017. Clinical diagnosis of progressive supranuclear palsy: The movement disorder society criteria. Mov. Disord. Off. J. Mov. Disord. Soc. 32, 853–864. https://doi.org/10.1002/mds.26987.
Hoover, B.R., Reed, M.N., Su, J., Penrod, R.D., Kotilinek, L.A., Grant, M.K., Pitstick, R., Carlson, G.A., Lanier, L.M., Yuan, L.-L., Ashe, K.H., Liao, D., 2010. Tau mislocalization to dendritic spines mediates synaptic dysfunction independently of neurodegeneration. Neuron 68, 1067–1081. https://doi.org/10.1016/j.neuron.2010.11.030.
Hornberger, M., Piguet, O., Graham, A.J., Nestor, P.J., Hodges, J.R., 2010. How preserved is episodic memory in behavioral variant frontotemporal dementia? Neurology 74, 472–479. https://doi.org/10.1212/WNL.0b013e3181cef85d.
Hornberger, M., Wong, S., Tan, R., Irish, M., Piguet, O., Kril, J., Hodges, J.R., Halliday, G., 2012. In vivo and post-mortem memory circuit integrity in frontotemporal dementia and Alzheimer's disease. Brain J. Neurol. 135, 3015–3025. https://doi.org/10.1093/brain/aws239.
Hughes, E.G., Peng, X., Gleichman, A.J., Lai, M., Zhou, L., Tsou, R., Parsons, T.D., Lynch, D.R., Dalmau, J., Balice-Gordon, R.J., 2010. Cellular and synaptic mechanisms of anti-NMDA receptor encephalitis. J. Neurosci. off. J. Soc. Neurosci. 30, 5866–5875. https://doi.org/10.1523/JNEUROSCI.0167-10.2010.
Humeau, Y., Reisel, D., Johnson, A.W., Borchardt, T., Jensen, V., Gebhardt, C., Bosch, V., Gass, P., Bannerman, D.M., Good, M.A., Hvalby, Ø., Sprengel, R., Lüthi, A., 2007. A pathway-specific function for different AMPA receptor subunits in amygdala long-term potentiation and fear conditioning. J. Neurosci. off. J. Soc. Neurosci. 27, 10947–10956. https://doi.org/10.1523/JNEUROSCI.2603-07.2007.
Hunter, D., Jamet, Z., Groc, L., 2021. Autoimmunity and NMDA receptor in brain disorders: where do we stand? Neurobiol. Dis. 147, 105161 https://doi.org/10.1016/j.nbd.2020.105161.
Italia, M., Ferrari, E., Diluca, M., Gardoni, F., 2022. NMDA and AMPA receptors at synapses: novel Targets for tau and α-synuclein proteinopathies. Biomedicines 10, 1550. https://doi.org/10.3390/biomedicines10071550.
Kertesz, A., Davidson, W., Fox, H., 1997. Frontal behavioral inventory: diagnostic criteria for frontal lobe dementia. Can. J. Neurol. Sci. J. Can. Sci. Neurol. 24, 29–36. https://doi.org/10.1017/s0317167100021053.
Kim, B.G., Dai, H.-N., McAtee, M., Vicini, S., Bregman, B.S., 2007. Labeling of dendritic spines with the carbocyanine dye DiI for confocal microscopic imaging in lightly fixed cortical slices. J. Neurosci. Methods 162, 237–243. https://doi.org/10.1016/j.jneumeth.2007.01.016.
Knopman, D.S., Kramer, J.H., Boeve, B.F., Caselli, R.J., Graff-Radford, N.R., Mendez, M. F., Miller, B.L., Mercaldo, N., 2008. Development of methodology for conducting clinical trials in frontotemporal lobar degeneration. Brain J. Neurol. 131, 2957–2968. https://doi.org/10.1093/brain/awn234.
Lai, M., Hughes, E.G., Peng, X., Zhou, L., Gleichman, A.J., Shu, H., Matà, S., Kremens, D., Vitaliani, R., Geschwind, M.D., Bataller, L., Kalb, R.G., Davis, R., Graus, F., Lynch, D. R., Balice-Gordon, R., Dalmau, J., 2009. AMPA receptor antibodies in limbic encephalitis alter synaptic receptor location. Ann. Neurol. 65, 424–434. https://doi.org/10.1002/ana.21589.
Li, Y., Ding, R., Ren, X., Wen, G., Dong, Z., Yao, H., Tan, Y., Yu, H., Wang, X., Zhan, X., Yao, J., Lu, Y., Zhang, G., Wu, X., 2019. Long-term ketamine administration causes tau protein phosphorylation and tau protein-dependent AMPA receptor reduction in the hippocampus of mice. Toxicol. Lett. 315, 107–115. https://doi.org/10.1016/j.toxlet.2019.08.023.
Li, J.-M., Li, X., Chan, L.W.C., Hu, R., Yang, S., 2023. A high fat diet in glutamate 3-/Y mice causes changes in behavior that resemble human intellectual disability. Physiol. Behav. 259, 114050 https://doi.org/10.1016/j.physbeh.2022.114050.
Mackenzie, I.R.A., Neumann, M., Bigio, E.H., Cairns, N.J., Alafuzoff, I., Kril, J., Kovacs, G.G., Ghetti, B., Halliday, G., Holm, I.E., Ince, P.G., Kamphorst, W., Revesz, T., Rozemuller, A.J.M., Kumar-Singh, S., Akiyama, H., Baborie, A., Spina, S., Dickson, D.W., Trojanowski, J.Q., Mann, D.M.A., 2010. Nomenclature and nosology for neuropathologic subtypes of frontotemporal lobar degeneration: an update. Acta Neuropathol. (berl.) 119, 1–4. https://doi.org/10.1007/s00401-009-0612-2.
Mantegazza, R., Bernasconi, P., Baggi, F., Spreafico, R., Ragona, F., Antozzi, C., Bernardi, G., Granata, T., 2002. Antibodies against GluR3 peptides are not specific for rasmussen's encephalitis but are also present in epilepsy patients with severe, early onset disease and intractable seizures. J. Neuroimmunol. 131, 179–185. https://doi.org/10.1016/s0165-5728(02)00261-8.
Matikainen-Ankney, B.A., Legaria, A.A., Pan, Y., Vachez, Y.M., Murphy, C.A., Schaefer, R.F., McGrath, Q.J., Wang, J.G., Bluitt, M.N., Ankney, K.C., Norris, A.J., Creed, M.C., Kravitz, A.V., 2022. Nucleus accumbens D1 receptor-expressing spiny projection neurons control food motivation and obesity. Biol. Psychiatry S0006–3223 (22), 01694–01698. https://doi.org/10.1016/j.biopsych.2022.10.003.
Maudes, E., Mannara, F., García-Serra, A., Radosevic, M., Mellado, A., Serafim, A.B., Planagumà, J., Sabater, L., Dalmau, J., Spatola, M., 2022. Human metabotropic glutamate receptor 5 antibodies Alter receptor levels and behavior in mice. Ann. Neurol. 92, 81–86. https://doi.org/10.1002/ana.26362.
Mellone, M., Zianni, E., Stanic, J., Campanelli, F., Marino, G., Ghiglieri, V., Longhi, A., Thiolat, M.-L., Li, Q., Calabresi, P., Bezard, E., Picconi, B., Di Luca, M., Gardoni, F., 2019. NMDA receptor GluN2D subunit participates to levodopa-induced dyskinesia pathophysiology. Neurobiol. Dis. 121, 338–349. https://doi.org/10.1016/j.nbd.2018.09.021.
Mendez-David, I., Guilloux, J.-P., Papp, M., Tritschler, L., Mocaer, E., Gardier, A.M., Bretin, S., David, D.J., 2017. S 47445 produces antidepressant- and anxiolytic-like effects through neurogenesis dependent and independent mechanisms. Front. Pharmacol. 8, 462. https://doi.org/10.3389/fphar.2017.00462.
Mikasova, L., De Rossi, P., Bouchet, D., Georges, F., Rogemond, V., Didelot, A., Meissirel, C., Honnorat, J., Groc, L., 2012. Disrupted surface cross-talk between NMDA and ephrin-B2 receptors in anti-NMDA encephalitis. Brain J. Neurol. 135, 1606–1621. https://doi.org/10.1093/brain/aws092.
Miller, E.C., Teravskis, P.J., Dummer, B.W., Zhao, X., Huganir, R.L., Liao, D., 2014. Tau phosphorylation and tau mislocalization mediate soluble aβ oligomer-induced AMPA glutamate receptor signaling deficits. Eur. J. Neurosci. 39, 1214–1224. https://doi.org/10.1111/ejn.12507.
Miyagawa, T., Brushaber, D., Syrjanen, J., Kremers, W., Fields, J., Forsberg, L.K., Heuer, H.W., Knopman, D., Kornak, J., Boxer, A., Rosen, H.J., Boeve, B.F., Appleby, B., Bordelon, Y., Bove, J., Brannelly, P., Caso, C., Coppola, G., Dever, R., Dheel, C., Dickerson, B., Dickinson, S., Dominguez, S., Domoto-Reilly, K., Faber, K., Ferrell, J., Fishman, A., Fong, J., Foroud, T., Gavrilova, R., Gearhart, D., Ghazanfari, B., Ghoshal, N., Goldman, J.S., Graff-Radford, J., Graff-Radford, N., Grant, I., Grossman, M., Haley, D., Hsiung, R., Huey, E., Irwin, D., Jones, D., Jones, L., Kantarci, K., Karydas, A., Kaufer, D., Kerwin, D., Kraft, R., Kramer, J., Kukull, W., Litvan, I., Lucente, D., Lungu, C., Mackenzie, I., Maldonado, M., Manoochehri, M., McGinnis, S., McKinley, E., Mendez, M.F., Miller, B., Multani, N., Onyike, C., Padmanabhan, J., Pantelyat, A., Pearlman, R., Petrucelli, L., Potter, M., Rademakers, R., Ramos, E.M., Rankin, K., Rascovsky, K., Roberson, E.D., Rogalski, E., Sengdy, P., Shaw, L., Tartaglia, M.C., Tatton, N., Taylor, J., Toga, A., Trojanowski, J.Q., Wang, P., Weintraub, S., Wong, B., Wszolek, Z., 2020. Utility of the global CDR® plus NACC FTLD rating and development of scoring rules: data from the ARTFL/LEFFTDS consortium. Alzheimers Dement. J. Alzheimers Assoc. 16, 106–117. https://doi.org/10.1002/alz.12033.
Monteiro-Fernandes, D., Silva, J.M., Soares-Cunha, C., Dalla, C., Kokras, N., Arnaud, F., Billiras, R., Zhuravleva, V., Waites, C., Bretin, S., Sousa, N., Sotiropoulos, I., 2021. Allosteric modulation of AMPA receptors counteracts tau-related excitotoxic synaptic signaling and memory deficits in stress- and aβ-evoked hippocampal pathology. Mol. Psychiatry 26, 5899–5911. https://doi.org/10.1038/s41380-020-0794-5.
Morley-Fletcher, S., Zuena, A.R., Mairesse, J., Gatta, E., Van Camp, G., Bouwalerh, H., Riozzi, B., Battaglia, G., Pittaluga, A., Olivero, G., Mocaer, E., Bretin, S., Nicoletti, F., Maccari, S., 2018. The reduction in glutamate release is predictive of cognitive and emotional alterations that are corrected by the positive modulator of AMPA receptors S 47445 in perinatal stressed rats. Neuropharmacology 135, 284–296. https://doi.org/10.1016/j.neuropharm.2018.03.018.
Palese, F., Bonomi, E., Nuzzo, T., Benussi, A., Mellone, M., Zianni, E., Cisani, F., Casamassa, A., Alberici, A., Scheggia, D., Padovani, A., Marcello, E., Di Luca, M., Pittaluga, A., Usiello, A., Borroni, B., Gardoni, F., 2020. Anti-GluA3 antibodies in frontotemporal dementia: effects on glutamatergic neurotransmission and synaptic failure. Neurobiol. Aging 86, 143–155. https://doi.org/10.1016/j.neurobiolaging.2019.10.015.
Peng, X., Hughes, E.G., Moscato, E.H., Parsons, T.D., Dalmau, J., Balice-Gordon, R.J., 2015. Cellular plasticity induced by anti-α-amino-3-hydroxy-5-methyl-4-isoxazolepropionic acid (AMPA) receptor encephalitis antibodies. Ann. Neurol. 77, 381–398. https://doi.org/10.1002/ana.24293.
Peng, S.-X., Pei, J., Rinaldi, B., Chen, J., Ge, Y.-H., Jia, M., Wang, J., Delahaye-Duriez, A., Sun, J.-H., Zang, Y.-Y., Shi, Y.-Y., Zhang, N., Gao, X., Milani, D., Xu, X., Sheng, N., Gerard, B., Zhang, C., Bayat, A., Liu, N., Yang, J.-J., Shi, Y.S., 2022. Dysfunction of AMPA receptor GluA3 is associated with aggressive behavior in human. Mol. Psychiatry 27, 4092–4102. https://doi.org/10.1038/s41380-022-01659-8.
Piccoli, G., Verpelli, C., Tonna, N., Romorini, S., Alessio, M., Nairn, A.C., Bachi, A., Sala, C., 2007. Proteomic analysis of activity-dependent synaptic plasticity in hippocampal neurons. J. Proteome Res. 6, 3203–3215. https://doi.org/10.1021/pr0701308.
Pilar-Cuellar, F., Castro, E., Bretin, S., Mocaer, E., Pazos, Á., Díaz, Á., 2019. S 47445 counteracts the behavioral manifestations and hippocampal neuroplasticity changes in bulbectomized mice. Prog. Neuropsychopharmacol. Biol. Psychiatry 93, 205–213. https://doi.org/10.1016/j.pnpbp.2019.04.005.
Prikas, E., Paric, E., Asih, P.R., Stefanoska, K., Stefen, H., Fath, T., Poljak, A., Ittner, A., 2022. Tau target identification reveals NSF-dependent effects on AMPA receptor

trafficking and memory formation. EMBO J. 41 https://doi.org/10.15252/embj.2021110242.e10242.

Rascovsky, K., Hodges, J.R., Knopman, D., Mendez, M.F., Kramer, J.H., Neuhaus, J., van Swieten, J.C., Seelaar, H., Dopper, E.G.P., Onyike, C.U., Hillis, A.E., Josephs, K.A., Boeve, B.F., Kertesz, A., Seeley, W.W., Rankin, K.P., Johnson, J.K., Gorno-Tempini, M.-L., Rosen, H., Prioleau-Latham, C.E., Lee, A., Kipps, C.M., Lillo, P., Piguet, O., Rohrer, J.D., Rossor, M.N., Warren, J.D., Fox, N.C., Galasko, D., Salmon, D.P., Black, S.E., Mesulam, M., Weintraub, S., Dickerson, B.C., Diehl-Schmid, J., Pasquier, F., Deramecourt, V., Lebert, F., Pijnenburg, Y., Chow, T.W., Manes, F., Grafman, J., Cappa, S.F., Freedman, M., Grossman, M., Miller, B.L., 2011. Sensitivity of revised diagnostic criteria for the behavioural variant of frontotemporal dementia. Brain J. Neurol. 134, 2456–2477. https://doi.org/10.1093/brain/awr179.

Regan, P., Mitchell, S.J., Kim, S.-C., Lee, Y., Yi, J.H., Barbati, S.A., Shaw, C., Cho, K., 2021. Regulation of synapse weakening through Interactions of the microtubule associated protein tau with PACSIN1. J. Neurosci. off. J. Soc. Neurosci. 41, 7162–7170. https://doi.org/10.1523/JNEUROSCI.3129-20.2021.

Sanchis-Segura, C., Borchardt, T., Vengeliene, V., Zghoul, T., Bachteler, D., Gass, P., Sprengel, R., Spanagel, R., 2006. Involvement of the AMPA receptor GluR-C subunit in alcohol-seeking behavior and relapse. J. Neurosci. off. J. Soc. Neurosci. 26, 1231–1238. https://doi.org/10.1523/JNEUROSCI.4237-05.2006.

Scheggia, D., Managò, F., Maltese, F., Bruni, S., Nigro, M., Dautan, D., Latuske, P., Contarini, G., Gomez-Gonzalo, M., Requie, L.M., Ferretti, V., Castellani, G., Mauro, D., Bonavia, A., Carmignoto, G., Yizhar, O., Papaleo, F., 2020. Somatostatin interneurons in the prefrontal cortex control affective state discrimination in mice. Nat. Neurosci. 23, 47–60. https://doi.org/10.1038/s41593-019-0551-8.

Scheggia, D., Stanic, J., Italia, M., La Greca, F., Zianni, E., Benussi, A., Borroni, B., Di Luca, M., Gardoni, F., 2021. GluA3 autoantibodies induce alterations in dendritic spine and behavior in mice. Brain. Behav. Immun. 97, 89–101. https://doi.org/10.1016/j.bbi.2021.07.001.

Stanic, J., Carta, M., Eberini, I., Pelucchi, S., Marcello, E., Genazzani, A.A., Racca, C., Mulle, C., Di Luca, M., Gardoni, F., 2015. Rabphilin 3A retains NMDA receptors at synaptic sites through interaction with GluN2A/PSD-95 complex. Nat. Commun. 6, 10181. https://doi.org/10.1038/ncomms10181.

Teravskis, P.J., Oxnard, B.R., Miller, E.C., Kemper, L., Ashe, K.H., Liao, D., 2021. Phosphorylation in two discrete tau domains regulates a stepwise process leading to postsynaptic dysfunction. J. Physiol. 599, 2483–2498. https://doi.org/10.1113/JP277459.

Walf, A.A., Frye, C.A., 2007. The use of the elevated plus maze as an assay of anxiety-related behavior in rodents. Nat. Protoc. 2, 322–328. https://doi.org/10.1038/nprot.2007.44.

Younes, K., Lepow, L.A., Estrada, C., Schulz, P.E., 2018. Auto-antibodies against P/Q- and N-type voltage-dependent calcium channels mimicking frontotemporal dementia. SAGE Open Med. Case Rep. 6, 2050313X17750928 https://doi.org/10.1177/2050313X17750928.